Results in Engineering 29 (2026) 109812

Contents lists available at ScienceDirect

Results in Engineering

journal homepage: www.sciencedirect.com/journal/results-in-engineering

Research paper

Blackberry leaf extract as a green inhibitor for copper corrosion: Insights from coordination complexes, thermodynamics, RSM optimization, and DFT calculations

Milica Zdravković [a,*], Robert Vianello [b,*], Vesna Grekulović [a], Nada Štrbac [a], Bojan Zdravković [c], Milan Gorgievski [a], Miljan Marković [a]

[a] Technical Faculty in Bor, University of Belgrade, Vojske Jugoslavije 12, Bor, Serbia
[b] Laboratory for the Computational Design and Synthesis of Functional Materials, Ruđer Bošković Institute, Zagreb, Croatia
[c] Serbia Zijin Mining D.O.O., Suvaja 185 A, Brestovac 19229, Serbia

ARTICLE INFO

Keywords:
Blackberry leaf
Copper
Organometallic complexes
Thermodynamic
RSM
Optimization
DFT calculations

ABSTRACT

This study provides a comprehensive evaluation of blackberry leaf extract (BLE) as a green inhibitor of copper corrosion in 0.5 M NaCl. The experimental method of gravimetric analysis was applied, the results of which were used for data analysis methods: adsorption and thermodynamic studies and statistical modeling. The density functional theory (DFT) method was applied to determine the influence on the process of corrosion inhibition by comparing BLE molecules and possible organometallic complexes formed between Cu ions in solution and BLE molecules. BLE, containing caffeic acid, quercetin-3-O-glucoside and kaempferol-3-O-glucoside, significantly reduced copper dissolution across 298–328 K, reaching inhibition efficiencie up to 99% at concentrations ≥10 g/L. Adsorption obeyed the Langmuir isotherm at all temperatures, and negative Gibbs free energies (–12.5 to –14.6 kJ/mol) confirmed spontaneous physical adsorption. The increase in activation energy and positive adsorption entropy values indicated an endothermic, physisorption-controlled process accompanied by water displacement from the copper surface. Response surface methodology showed excellent predictive power ($R^2 >$ 0.97), identifying inhibitor concentration as the most influential factor, followed by immersion time and temperature. Optimization predicted conditions yielding 99% inhibition, validated experimentally. DFT calculations established the stability and preferred geometries of Cu(II) complexes formed with the main BLE constituents, supporting their participation in adsorption, which represents a significant novelty in relation to previous research on plant corrosion inhibitors. Overall, the combined experimental-computational approach confirms BLE as a highly efficient, eco-friendly solution for copper protection in chloride environments.

1. Introduction

The integrity and safety of machinery and equipment are strongly affected by metal corrosion, which compromises production buildings, work platforms and metal pipelines. In addition, corrosion leads to environmental pollution and significantly reduces the service lifetime of equipment operating in aggressive environments [1]. Copper and copper-based alloys are a widely used engeneering metal, but it is susceptible to corrosion under specific conditions [2]. A typical example is the marine industry, where copper is exposed to aggressive chloride ions [3]. Corrosion in such environment represents a major challenge. Therefore, it is of utmost importance to find effective methods to prevent corrosion. Common methods for corrosion prevention in seawater include corrosion inhibitors, cathodic protection, and protective coatings [4]. In earlier research, plant inhibitors were shown to be effective inhibitors of copper corrosion in various corrosive environments, with *Benincasa Hispida* leaf extract [1], Eupatorium adenoprum leaves extract [5], *Alchemilla Vulgaris* extract [6], *Leucas aspera* leaves extract [7], Jujube shell extract [8] and Egyptian licorice extract [9] used as inhibitors. Among these, corrosion inhibitors are particularly attractive due to their ease of application, relatively low cost and high efficiency [1]. Ideally, the corrosion inhibitor requires simple preparation methods, favorable water solubility, practical significance and research value [5,10].

* Corresponding authors.
E-mail addresses: mboskovic@tfbor.bg.ac.rs (M. Zdravković), robert.vianello@irb.hr (R. Vianello).

https://doi.org/10.1016/j.rineng.2026.109812
Received 9 January 2026; Received in revised form 16 February 2026; Accepted 26 February 2026
Available online 6 March 2026

Previous research has shown that blackberry (*Rubus fruticosus* L.) leaf extract (BLE) in 0.5 M NaCl solution proved to fulfill these criteria as an efficient green inhibitor for copper corrosion. Electrochemical studies (potentiodynamic polarization, electrochemical frequency modulation and electrochemical impedance spectroscopy) show that BLE acts as a mixed-type inhibitor, with extract molecules physically adsorbing onto the copper surface and mitigating the aggressive action of chloride ions. The adsorption process follows the Langmuir adsorption isotherm. The lowest value of the corrosion rate was achieved with the addition of 15 g/L BLE after 10 days at room temperature with an inhibition efficiency of 99.1%, in which the gravimetric method was applied with an immersion time of 3 to 10 days. At BLE lower than 15 g/L, the corrosion process is diffusion-controlled, whereas at 15 g/L it is governed by charge transfer, which was determined by electrochemical impedance spectroscopy. Although there is an indication that there is a change in the corrosion inhibition mechanism at concentrations higher than 10 g/L, there is no explanation in previous research as to why the change occurs. HPLC–DAD analysis identified caffeic acid, quercetin-3-O-glucoside, and kaempferol-3-O-glucoside as the main constituents of BLE, while their functional groups were characterized by ATR-FTIR spectroscopy. UV–Vis absorption spectra confirmed the formation of complexes between copper ions and extract molecules, while SEM-EDS analysis verified the adsorption of BLE molecules onto the copper surface, confirming their inhibitive role [11,12]. In addition, by applying the UV–Vis method, it was determined that at a concentration of 5 g/L BLE and 10 g/L BLE, the formation of organometallic complexes of copper and organic compounds present in BLE does not occur [13].

To obtain a deeper understanding of the inhibition mechanism of BLE under chloride conditions, further detailed investigations are required. Owing to the complexity of the corrosion system, which involves numerous molecules and possible interactions between sodium chloride and BLE components, it is important to determine the pH and electrical conductivity of the solution prior to copper immersion. Subsequently, the manner in which BLE protects the copper surface from chloride ions at both low and high inhibitor concentrations should be systematically examined. Such an approach allows the reactions occurring in this complex system to be inferred based on existing literature and experimental observations, as well as to assess whether any of the resulting species could pose a potential risk to the environment, despite BLE being a natural plant extract. In addition, this type of analysis contributes to broader knowledge in areas beyond corrosion science, particularly regarding the formation of organometallic complexes of copper with caffeic acid, quercetin-3-O-glucoside, and kaempferol-3-O-glucoside, for which comprehensive data are still lacking in the literature.

Because the primary goal of using plant-based corrosion inhibitors is to replace toxic conventional inhibitors, a dedicated subsection entitled Possible reactions of complex formation was introduced to demonstrate that the products formed before and after copper corrosion inhibition by BLE do not exert harmful effects on living organisms. As this type of mechanistic representation is rarely addressed in the literature, it can facilitate future studies and improve understanding of systems involving plant-based inhibitors. Furthermore, whereas previous studies of BLE as a copper corrosion inhibitor in 0.5 M NaCl solution were limited to room temperature and immersion times up to 10 days, the present work extends gravimetric analysis to different temperatures. This enables determination of the thermodynamic parameters governing copper corrosion in chloride media in the presence of BLE and represents an additional novelty of this study.

In addition to the classical electrochemical and chemical methods that can be used to study the effect of corrosion inhibitors, more recent research has focused on computer modeling and process optimization to determine the simultaneous influence of multiple parameters that affect corrosion and the conditions under which the corrosion inhibitor works best [14,15]. Response surface methodology (RSM), process optimization, DFT and molecular dynamics (MD) simulations proved its usefulness [15–18]. Statistical tools for experimental design, such as the RSM (Response Surface Methodology), enable the prediction and optimization of the investigated processes [19]. By applying this method and laboratory experiments, it is possible to determine the simultaneous influence of parameters that affect the process under study. This method can be used to determine under which conditions the corrosion inhibitor works best, and the optimization of the corrosion process with the inhibitor is usually carried out with the change in temperature, time of immersion of the metal in the electrolyte and corrosion inhibitor concentration [20]. Inhibitor and electrolyte concentrations, and the time of immersion of the metal in the electrolyte can also be taken as a combination of variables [21–23]. By optimizing the corrosion process, it is possible to determine at which parameters the highest percentage inhibitory effect is achieved with the minimum dose of corrosion inhibitor, while investigating the simultaneous effect of several parameters [24]. The most commonly applied models used in the response surface methodology are the full factorial design (FFD) [19], the Box-Behnken design (BBD) [25] and the central composite design (CCD) [21]. By utilizing RSM, it is possible to create a model that can be used to predict the value of mass loss, corrosion rate and the effectiveness of corrosion inhibitors. When creating the model, it is necessary to determine whether the actual and predicted values match and whether the model is statistically significant in predicting the specified values [23]. Identifying the optimal combination of temperature, immersion time and inhibitor concentration for BLE in 0.5 M NaCl, as well as the statistical significance of each parameter, is essential for practical application.

Although the presence of copper-extract complexes in solution has been experimentally observed at a BLE concentration of 15 g/L, their preise nature and stoichiometry remain unresolved. Therefore, computational density functional theory (DFT) calculations, supported by literature data on copper-flavonoid organometallic complexes involving caffeic acid, quercetin-3-O-glucoside, and kaempferol-3-O-glucoside, are required to elucidate the possible complex structures [12]. This data is very valuable, as the existing literature on plant-based corrosion inhibitors rarely addresses which specific copper complexes may form in solution or whether these complexes actively participate, alongside inhibitor molecules, in the adsorption process on the metal surface.

By determining the pH and conductivity of a 0.5 M NaCl solution both with and without the addition of BLE prior to copper introduction, identifying possible reactions in this complex system where corrosion inhibition occurs in the presence of BLE molecules and their organometallic complexes, and experimentally evaluating the effects of temperature on the corrosion inhibition process, as well as the combined effects of temperature, immersion time, and BLE concentration on corrosion, this study contributes to previous research on BLE as a copper corrosion inhibitor in chloride environments. An additional scientific contribution is the determination of the optimal temperature, immersion time, and BLE concentration at which BLE exhibits maximal inhibitory activity. The main novelty lies in the identification of organometallic complexes formed between copper ions in solution and BLE molecules. Notably, prior literature on plant-based corrosion inhibitors has not included DFT analyses of possible complexes formed between metal ions and plant inhibitor molecules.

2. Experimental

2.1. Materials and sample preparation

Blank solution and blackberry leaf extract (BLE) were prepared in line with our recent report [12]. The solutions with BLE addition contained different BLE concentrations of 2 g/L, 5 g/L, 10 g/L, 15 g/L. In addition to the mentioned electrolyte concentrations with the addition of BLE, solutions with concentrations of 18.4090 g/L and 1.5910 g/L BLE were prepared for the RSM experiments. To test the corrosion inhibition efficiency value of 99% obtained by the optimization process, a

solution with a concentration of 15 g/L BLE was used.

2.2. The pH value of the electrolyte and the electrolytic conductivity

The determination of the electrolyte pH value, i.e. the 0.5 M NaCl solution without and with the addition of BLE (2 - 15 g/L), was carried out at room temperature. The Vision Plus pH6175, manufactured by Jenco Instruments, USA, was used for pH measurement. The Cond 720, WTW InoLab, Germany, was used to measure the electrolytic conductivity of the electrolyte.

2.3. Gravimetric study

The gravimetric experiments were performed with copper coupons (1 cm x 1 cm) made of Cu-DHP copper sheet (99.9000% Cu, 0.0198% P, 0.0005% Pb). The coupons were polished, cleaned with acetone and distilled water and dried. The mass of the coupons was measured with an analytical balance (AS 220.R2, Radwag wagi elektroniczne, Poland) with an accuracy of 10^{-4} g and then immersed in the solutions. To investigate the temperature effect on the copper corrosion process in a 0.5 M NaCl solution with and without the addition of BLE (2 g/L, 5 g/L, 10 g/L and 15 g/L), the mass of the copper plate was measured before and after leaving it in the electrolyte for 3 days at different temperatures (298 K, 308 K, 318 K, 328 K). Each experiment was performed with three copper samples. Each copper coupon was immersed in 10 mL of electrolyte in a test tube with a stopper to prevent the electrolyte from evaporating during standing and temperature changes. The test tubes were immersed in a laboratory beaker containing distilled water and a thermostat acting directly on the heating plate to maintain a constant temperature. The temperature was achieved and maintained using a magnetic stirrer with heating and a ceramic heating plate (C-MAG HS 7 – IKA, Werke GmbH & Co). All three test tubes were treated under the same conditions, so that after cleaning the plates and calculating the mass difference after and before the experiment, it was determined whether there was a deviation in the value between the three coupons. In this way, errors in the experimental procedure were avoided and valid values were taken into account.

The corrosion rate (CR) was calculated using the following equation [20]:

$$CR = \frac{m_1 - m_2}{(S \cdot t)} \tag{1}$$

The degree of surface coverage was calculated using the equation [20]:

$$\theta = \frac{CR_0 - CR}{CR_0} \tag{2}$$

where m_1 is the weight of the copper coupon before corrosion, m_2 is the weight of the copper coupon after corrosion, S is the surface area of the copper coupon (cm^2), t is the time (h), CR_0 and CR are the corrosion rates in (g $h^{-1}cm^{-2}$) without and with BLE, respectively.

Monitoring the temperature variation allows the characterization of the electrochemical system without and with the addition of an inhibitor to determine the type of adsorption, process spontaneity, the adsorption mechanism, and the inhibitor behavior at elevated temperatures [26,27]. The adsorption type is determined by the value of the change in Gibbs free energy of adsorption calculated from the following equations [6,11,28,29]:

$$\Delta G_{ads}^{\circ} = -RTlnK \tag{3}$$

$$K = \frac{\theta}{C_{inh}}(1-\theta) \tag{4}$$

$$\Delta G_{ads}^{\circ} = -RTln(55,5K) \tag{5}$$

where ΔG_{ads}° is the change in Gibbs free energy of adsorption, R is the universal gas constant, T is the temperature, K is the adsorption constant, θ is the degree of surface coverage, and C_{inh} is the concentration of the inhibitor. A value representing the molar concentration of water was added to the adsorption constant 55.5.

The value of ΔG_{ads}° up to –20 kJ/mol or less exergonic, indicates that the inhibitor adsorption onto the metal surface occurs through electrostatic interactions between charged molecules and metal ions, implying the physical inhibitor adsorption. When the ΔG_{ads}° value exceeds –40 kJ/mol, a chemical adsorption occurs involving the inhibitor-metal surface charge transfer [6,30–32]. In general, the negative value of ΔG_{ads}° indicates that the adsorption occurs spontaneously [33].

The Van Hoff Eq. (6), the Gibbs-Helmholtz Eq. (7) and the basic equation of thermodynamics (8) were used to determine the thermodynamic parameters of the corrosion process. The enthalpy change is calculated using the Van Hoff equation [34,35]:

$$lnK_{ads} = -\frac{\Delta H_{ads}^{o}}{RT} + \frac{\Delta S_{ads}^{o}}{R} + ln\frac{1}{55,5} \tag{6}$$

The slope value for $\frac{\Delta H_{ads}^{o}}{R}$ was obtained from the plot of K_{ads} vs. $1/T$. The adsorption entropy is calculated on the axis of the segment function obtained by the Van Hoff equation [35]. The attained adsorption enthalpy can be compared with that from the Gibbs-Helmholtz equation:

$$\left[\frac{\partial\left(\Delta G_{ads}^{o}/T\right)}{\partial T}\right] = -\frac{\Delta H_{ads}^{o}}{T^2} \tag{7}$$

where $\Delta G_{ads}^{o}/T$ relative to the $1/T$ slope is equal to ΔH_{ads}^{o}. The values of the adsorption enthalpy and the adsorption entropy can also be determined using the basic equation of thermodynamics [34,35]:

$$\Delta G_{ads}^{\circ} = \Delta H_{ads}^{O} - T\Delta S_{ads}^{O} \tag{8}$$

where the slope of the function is equal to $-\Delta S_{ads}^{O}$, and the intercept is ΔH_{ads}^{O}.

The entropy change in the system ΔS_{ads}^{O} is mostly positive in the presence of the inhibitor, suggesting that the active complex formation represents the rate-limiting step. Moreover, it indicates association rather than dissociation, indicating that disorder is reduced by reactants complex formation [36]. Furthermore, it can be concluded from thermodynamic principles that adsorption itself is an exothermic process accompanied by a decrease in entropy [34,37]. The standard values of activation enthalpy and entropy can be calculated using the equation derived from the theory of transition states [8]:

$$log\left(\frac{CR}{T}\right) = \left[log\left(\frac{R}{Nh}\right) + \left(\frac{\Delta S^{O}}{2,303R}\right)\right] - \frac{\Delta H^{O}}{2,303RT} \tag{9}$$

where CR is the corrosion rate, N is the Avogadro number, h is Planck constant, ΔS^{O} is the standard entropy change, ΔH^{O} is the standard enthalpy change.

The corrosion rate is calculated using the Arrhenius equation [34,38]:

$$logCR = -\frac{E_a}{2,303RT} + A \tag{10}$$

where Ea is the activation energy and A is the Arrhenius constant.

The activation energy (Ea) of the corrosion process is obtained from the slope of the Arrhenius plot. An increase in Ea in the presence of an inhibitor compared to the uninhibited system indicates spontaneous adsorption of inhibitor molecules on the metal surface and is commonly associated with a physisorption-controlled inhibition mechanism [8,9,39]. A higher activation energy in the inhibited system also implies a reduction in the number of available active sites on the metal surface, thereby decreasing the effective area over which corrosion can occur [34]. This increase in Ea reflects a modification of the corrosion pathway

caused by the presence of inhibitor molecules, indicating a change in the underlying corrosion mechanism relative to the blank solution [40].

It is also necessary to determine the adsorption isotherm governing inhibitor adsorption at elevated temperatures in order to verify whether the adsorption behavior remains consistent with that observed at room temperature. Analysis of the adsorption isotherm provides valuable insight into the nature of the interaction between the corrosion inhibitor and the metal surface. Determination of the appropriate adsorption isotherm requires knowledge of the surface coverage degree (θ), which is calculated using the following expression [31]:

$$\theta = \frac{IE}{100} \tag{11}$$

where *IE* is the inhibition efficiency.

The most commonly used adsorption isotherms are the Langmir, Frumkin, Temkin, Freundlich, Florey-Huggins and El-Awadi isotherms [41,42], and De Boer, Parson and Bokris-Swinkels [33,43–45]. Since the Langmire adsorption isotherm was found to be a suitable isotherm for the adsorption of BLE on the copper surface at room temperature, it was necessary to check whether this adsorption isotherm corresponds to the corrosion inhibition process at elevated temperatures. The formula for the Langmire adsorption isotherm is:

$$\frac{C_{inh}}{\theta} = \frac{1}{K_{ads}} + C_{inh} \tag{12}$$

where C_{inh} is the concentration of the corrosion inhibitor.

2.4. RSM and optimization of the corrosion inhibition process

The response surface methodology was used to determine the synergistic effect of temperature, residence time of copper in the electrolyte and BLE concentration on the Cu-DHP copper corrosion inhibition process. The independent variables were designated as follows: A: immersion time of copper in 0.5 M NaCl solution with the addition of different inhibitor concentrations (Xa), B: temperature (Xb) and C: inhibitor concentration (Xc). The corrosion rate (Y1) and the percentage of inhibition efficiency (Y2), which were determined using the weight loss method, were entered as responses (dependent variables). The coded and uncoded values of the independent variables are shown in Table 1. A wide range of BLE concentrations was selected to cover the range above which the adsorption mechanism changes. This choice is based on earlier results obtained using the EIS method, where the same BLE concentration range was applied, as described in the Introduction. No experiments were performed at concentrations below 2 g/L to avoid negative inhibitor concentrations in the RSM-CCD model. Based on the studies presented in the Introduction, an immersion time of 3 to 10 days was chosen, allowing the RSM results to be compared with research using the gravimetric analysis with varying immersion times [11]. In order to determine whether there is a possible deviation of the behavior of BLE as a corrosion inhibitor, an appropriate number of axial points were used, which are different for the alpha value compared to the previously applied inhibitor concentration values (1.5910 g/L BLE and 18.4090 g/L) and immersion time. The temperature range was set according to commonly reported values in the literature for thermodynamic studies of corrosion processes using metal corrosion inhibitors.

RSM is a method of designing experiments that is achieved by applying mathematical and statistical methods to obtain a mathematical model that meets statistical parameters such as the F-test and the p-value (statistical significance level). In this way, it is possible to determine how the dependent parameters (variables) decrease as the independent variables change [24]. The statistical significance of the individual variables and the model was tested using analysis of variance (ANOVA). The model is a full two-level face-centered CCD, where α = 1.68179, with three factors, 8 cube points, 6 central points and 6 axial points were used to create the model. Based on the number of points, a model with 20 experiments was formed. The software Minitab 19 (Minitab Statistical Software) was used. To avoid systematic errors, the experiments were randomly assigned. The results were analyzed by multiple regression, considering the coefficients by analysis of variance and the significance level p ($p \leq 0.05$) [24,46]. The quality of the model was determined using the value of the coefficient of determination and the adjusted coefficient of determination (R^2 and R^2 (adj)). Statistical significance was determined using the Fisher test (F-test) [24,47]. Contour plots with two variables and 3D surface plots are displayed as results of the RSM. In this way, it is easy to see under which conditions blackberry leaf extract works best as a copper corrosion inhibitor Cu-DHP in 0.5 M NaCl.

Optimization of the BLE copper inhibition process was applied to determine under which conditions BLE works best. Since the experiments presented in previous publications were carried out with the influence of one parameter on the corrosion process, by applying the optimization procedure it is possible to test the simultaneous effect of several parameters, thus achieving more realistic conditions that can be applied in practice. In order to determine the optimal parameters for the process of copper corrosion inhibition by Cu-DHP in 0.5 M NaCl using BLE, the maximum percentage of inhibition efficiency was determined using the RSM model. Previous studies indicate some shortcomings and limitations in the application of RSM, such as the impossibility of extrapolation and prediction only in a certain range of factors [24]. The response surface methodology and process optimization were applied after the weight loss method, determination of adsorption and thermodynamic parameters and extrapolation to match the range of factors with the change in mechanism and avoid possible errors.

Table 1
Experimental values of the independent variables.

Independent variables	Coded values	
	−1	1
Time (h)	72	240
Temperature (K)	303	328
Inhibitor concentration (g/L)	5	15

2.5. Computational DFT analysis

The intial set of molecular geometries for individual ligands and their Cu(II) complexes was obtained using the Conformer-Rotamer Ensemble Sampling Tool (CREST) [48]. CREST calculations use the GFN2-xTB tight binding Hamiltonian [49], the generalized Born with surface area contributions (GBSA) continuum model for water solvent [50], and the iMTD-GC metadynamics-based exploration of conformational space for the collective variables [51]. The ten distinct lowest-energy conformations generated by CREST were used as starting points for the DFT geometry optimization employing the M06–2X/def2-TZVP model, known to be successful in reproducing geometries, dipole moments, and homolytic bond energies in various metal complexes [52]. The most stable structures following this DFT protocol were used for the analysis. To account for the effect of the water solution, during geometry optimization, we included the implicit SMD solvation model, as employed in our earlier studies [53–55]. Thermal corrections were extracted from the corresponding frequency calculations, so that all of the presented results correspond to differences in the Gibbs free energies at room temperature. All calculations were performed using the Gaussian 16 software [56].

3. Results and discussion

3.1. The pH value of the electrolyte and the electrolytic conductivity

The results of measuring the pH and electrolytic conductivity (γ) of the electrolyte for copper corrosion tests in a 0.5 M NaCl solution

without and with the addition of different BLE concentrations are shown in Table 2.

The main corrosion products of copper in NaCl solution in acidic to neutral environment are $CuCl_2^-$ or Cu^{2+} at certain potential values determined based on the E-pH diagram, while in alkaline environment (pH~7–14) they are Cu_2O and CuO [57]. Considering the pH values given in Table 2 and the literature results, the most common corrosion product in 0.5 M NaCl solution is $CuCl_2^-$. The research results of different concentrations and pH values of NaCl solution on copper corrosion show that the most corrosive environment is a highly concentrated solution (5 M NaCl), with a pH value of around 7. The same study shows that the macro changes, i.e. the value of the corrosion potential, are more influenced by the change in pH than by the change in the concentration of the NaCl solution [57]. The results of the pH of the 0.5 M NaCl solution in the presence of BLE show a decrease in pH with increasing BLE concentration, indicating an environment that has a lower corrosive effect on copper Cu-DHP.

The electrolytic conductivity of the solution is slightly reduced in the presence of BLE at concentrations ranging from 2 to 10 g/L compared to the uninhibited 0.5 M NaCl solution. At a BLE concentration of 15 g/L, a small increase in conductivity is observed relative to the lower extract concentrations. This trend is consistent with changes in electrolyte resistance determined by electrochemical impedance spectroscopy (EIS) [12]. An increase in electrolyte resistance corresponds to a decrease in ionic transport through the solution, whereas higher electrolytic conductivity generally promotes higher corrosion rates due to enhanced charge transfer processes [58]. The observed variations in both pH and electrolytic conductivity therefore support the inhibitive effect of BLE on copper corrosion in 0.5 M NaCl.

3.2. Possible reactions of complex formation

Each of the three main BLE compounds (caffeic acid, quercetin-3-O-glucoside and kaempferol-3-O-glucoside), determined by HPLC, can potentially react with the ions present in the electrolyte. The reactions that take place in the copper-electrolyte system, where the electrolyte is a 0.5 M NaCl solution without and with the addition of BLE, can be divided into three groups. The first group involve reactions in the electrolyte before the copper is immersed in the electrolyte, in which BLE compounds can react with sodium and chlorine ions. The second group are the reactions between copper and 0.5 M NaCl solution without the addition and the third group are those between copper and the 0.5 M NaCl solution under the different BLE concentrations.

The available research on the reactions between antioxidants and sodium and chlorine ions is mainly focused on the biological effects of these compounds. Sodium chloride solution is usually administered to patients when testing the effect of natural preparations containing quercetin-3-O-glucoside and kaempferol-3-O-glucoside, as sodium is thought to enable the active glucose transport and quercetin adsorption in the body [59,60]. A direct reaction of BLE components with chlorine ions in the 0.5 M NaCl solution would be feasible if a suitable oxidizing agent is present. This phenomenon is explained by the electrophilic reagent formation (Br^+, Cl^+) by the oxidation in the environment. Earlier reports suggest that halogens improve the effect of organic corrosion inhibitors, with the synergistic effect following the order: $I^- > Br^- > Cl^-$. Their effect can be explained by two mechanisms and is based on the formation of an ion pair from a halide ion and an organic molecule [61–63].

Table 2
pH and electrolytic conductivity values of the 0.5 M NaCl solution with and without the addition of BLE at room temperature.

C_{inh} (g/L)	pH	γ (μS/cm)
0	6.16	49.9
2	5.83	45.0
5	5.66	45.0
10	5.59	45.0
15	5.57	46.2

Corrosion of Cu-DHP copper in a 0.5 M NaCl solution leads to the transfer of copper ions into the solution, which can form a complex with BLE components, as confirmed by UV–Vis spectra [11], yet their precise nature remains undetermined. The interaction among flavonoids and electrolyte complexity must be considered, in which OH^- and H^+ ions, H_2O molecules and organics are present together with Na^+ and Cl^-. A synergistic effect can occur, as in the case of kaempferol and myricetin, but also the opposite effect, as in the case of quercetin and myricetin [64]. A large number of studies have shown that flavonoids can form high-affinity complexes with transition metals such as copper and iron [65–70]. Copper chloride is often used as a starting substance for the formation of organometallic complexes [70]. Since copper chlorides are present as a corrosion product of copper in a 0.5 M NaCl solution as well as Cu(II) ions based on the E-pH diagram, it is clear that the formation of an organometallic complex can occur in a solution with the addition of BLE [11,71].

Studies on the effect of mineral supplements on flavonoid glucosides showed that a complex is formed between copper ions and quercetin glucosides [72]. The stability of the complex of divalent metal ions of quercetin decreases in the following order: Cu (II) > Ni (II) > Co (II) > Fe (II) > Zn (II). The stoichiometry of metals and flavonoids is 2:1 in the case of the formation of complexes with Fe (II), Ni (II), Co (II) and Zn (II), while for Cu (II) the mechanism is different due to simultaneous oxidation, partly because Cu (II) has stronger oxidative activity and because quercetin is more easily oxidized under acidic conditions [72,73]. In solutions with pH = 5.5–6.8, as with BLE in 0.5 M NaCl solution, the formation of various copper complexes and quercetin 3-O-glucoside occurs [74]. When a 1:1 complex is formed, the reaction occurs via the carbonyl oxygen and the 3-OH group on the C-ring [75]. Based on the literature data and the pH results, the Cu^{1+} ion complex with quercetin-3-O-glucoside most likely does not occur, but that the Cu^{2+} complex is formed, whose stability increases with BLE concentrations [11,74].

Quercetin differs from kaempferol by an additional -OH group on the B-ring (at position 3), so that the comparison of these two favonoids and their derivatives is often made in the form of organometallic complexes. Kaempferol–Cu(II) complexes have been studied for their antioxidant and prooxidant behaviour, but the existence of two stoichiometries (1:1 and 1:2) has also been noted [76]. The formation of this complex in a pure NaCl solution was not reported, as the influence of biologically significant metals on kaempferol and its derivatives is important for their effect in human serum [77]. Various mechanisms are involved in the formation of caffeic acid complexes with metals. The resulting product inhibits the formation of free radicals and can have an indirect effect on the living world by influencing metabolic reactions [78]. Research confirms the formation of caffeic acid complexes with Cu^{2+} in NaCl solution [78]. This means that the copper ions formed during Cu-DHP copper corrosion in the 0.5 M NaCl solution can react with caffeic acid, allowing the resulting product to interact with the copper surface. The stability of complexes formed from caffeic acid and metal is well known and can be illustrated as follows: $Zn^{2+\langle}$ $Cu^{2+\rangle}$ Cd^{2+} [79]. Based on the stability ~~diagram~~ of various caffeic acid complexes with Cu^{2+} ions [78] and the pH of the 0.5 M NaCl solution without and with the addition of BLE, in the range $3 \leq pH \leq 6$, it is possible to determine which types of complexes are present. The following types are dominant: $M_2LH_2^{3+}$, M_2LH_2 i $M_2L_2^0$. The second site of the benzene ring of caffeic acid is the most electrophilic site, therefore the reaction with nucleophilic species can occur there [80].

Also, the group of reactions in the 0.5 M NaCl solution without and with BLE is represented by the corrosion reactions and were explained by electrochemical analysis [11,12]. The adsorption capacity of heterocyclic compounds depends on the charge of the metal surface, the

temperature and the residence time of the metal in the electrolyte [81, 82]. The influence of these parameters on BLE adsorption on the copper surface in the 0.5 M NaCl solution was investigated using the weight loss method and the response surface methodology, the results of which are presented in this paper.

3.2.1. The weight loss method at different temperatures

Based on the results of measuring the mass change of copper in a 0.5 M NaCl solution without and with the addition of BLE (2 g/L - 15 g/L) at different temperatures after standing in the electrolyte for three days, the influence of temperature on the copper corrosion process in the presence of chloride ions and the adsorption of BLE on the copper surface at different temperatures was determined. Table 3 shows the measurement results, where the difference between the mass before and after the experiment (Δm) is given as the copper mass change during standing in the electrolyte for a period of 3 days at different temperatures, as well as the temperatures at which the experiments were conducted (T), the surface coverage degree (θ), the corrosion rate (CR) and the inhibition efficiency percentage (IE). The IE value was calculated based on the value of the degree of coverage and applying Eq. (11).

The results show that after standing the copper in the electrolyte for 3 days, the value of the corrosion rate increases with increasing temperature both in the 0.5 M NaCl solution without the addition of BLE and in the 0.5 M NaCl solution with the different concentrations of BLE. At all temperatures, there is a significant reduction in the copper corrosion rate at a constant temperature in the presence of BLE compared to the value of the copper corrosion rate in the solution without the additive. The BLE corrosion inhibition values decrease slightly with increasing temperature at all BLE concentrations. The decrease in BLE corrosion inhibition efficiency with increasing temperature indicates that physical adsorption of the inhibitor molecules on the copper surface occurs [83]. The highest corrosion rate value is $5.76{\cdot}10^{-5}$ g/h·cm^2 for the solution without BLE at the highest temperature (328 K). The lowest value for the corrosion rate is 6.94·10–7 g/h·cm^2 at 15 g/L BLE, at 298 K, with an inhibition efficiency of 98.33%. To better understand the influence of temperature on the copper corrosion process in a 0.5 M NaCl solution without and with BLE addition, an Arrhenius plot and a transition state diagram were generated and then the activation parameters were calculated.

Fig. 1 shows a diagram of the dependence of the copper corrosion rate in a 0.5 M NaCl solution with the addition of BLE (2 g/L – 15 g/L) at

Table 3
Cu-DHP mass loss (Δm) at different electrolyte temperatures, degree of surface coverage (θ), corrosion rate (CR) and percentage inhibition efficiency (IE) as a function of different inhibitor concentrations (Cinh) and electrolyte temperature (T), after 3 days.

T (K)	C_{inh} (g/L)	Δm (g)	CR (g/h·cm^2)	θ	IE (%)
298	0	0.0060	$4.16{\cdot}10^{-5}$	-	-
	2	0.0006	$4.16{\cdot}10^{-6}$	0.9000	90.00
	5	0.0005	$3.47{\cdot}10^{-6}$	0.9167	91.67
	10	0.0003	$2.08{\cdot}10^{-6}$	0.9500	95.00
	15	0.0001	$6.94{\cdot}10^{-7}$	0.9833	98.33
308	0	0.0067	$4.65{\cdot}10^{-5}$	-	-
	2	0.0007	$4.86{\cdot}10^{-6}$	0.8955	89.55
	5	0.0006	$4.17{\cdot}10^{-6}$	0.9105	91.05
	10	0.0004	$2.78{\cdot}10^{-6}$	0.9403	94.03
	15	0.0002	$1.39{\cdot}10^{-6}$	0.9701	97.01
318	0	0.0074	$5.14{\cdot}10^{-5}$	-	-
	2	0.0008	$5.56{\cdot}10^{-6}$	0.8919	89.19
	5	0.0007	$4.86{\cdot}10^{-6}$	0.9054	90.54
	10	0.0005	$3.47{\cdot}10^{-6}$	0.9324	93.24
	15	0.0003	$2.08{\cdot}10^{-6}$	0.9595	95.95
328	0	0.0340	$5.76{\cdot}10^{-5}$	-	-
	2	0.0009	$6.25{\cdot}10^{-6}$	0.8916	89.16
	5	0.0008	$5.56{\cdot}10^{-6}$	0.9036	90.36
	10	0.0006	$4.17{\cdot}10^{-6}$	0.9277	92.77
	15	0.0004	$2.28{\cdot}10^{-6}$	0.9518	95.18

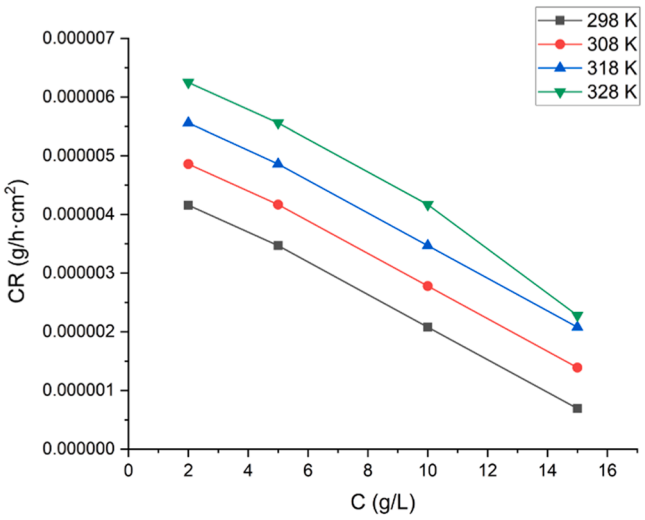

Fig. 1. Change in the copper corrosion rate of Cu-DHP in a 0.5 M NaCl solution with the addition of BLE (2 g/L - 15 g/L) at different temperatures.

different temperatures. The corrosion rate decreases with increasing BLE concentration [84]. The dependence of copper corrosion inhibition in 0.5 M NaCl on BLE concentration at different electrolyte temperatures is shown in Fig. 2. The change in inhibition efficiency was lower at lower BLE concentrations, but at the same temperatures, the value of inhibition efficiency was higher with increasing BLE concentration. The highest values of inhibition efficiency were obtained at the lowest temperature.

3.3. Adsorption isotherms at different temperatures

The influence of the temperature change from 298 K to 328 K on the copper corrosion process in a 0.5 M NaCl solution with the different concentrations of BLE was investigated by means of adsorption isotherms, using the data from Table 3. The Langmuir adsorption isotherm corresponds to the BLE adsorption on the copper surface determined by the high value of the correlation coefficient: 0.999326 (298 K), 0.99945 (308 K), 0.999538 (318 K) and 0.999632 (328 K). In this way, it was confirmed that the adsorption of the inhibitor takes place in an active site and that there are no interactions between the adsorbed molecules when the temperature changes [85]. Based on the adsorption isotherms,

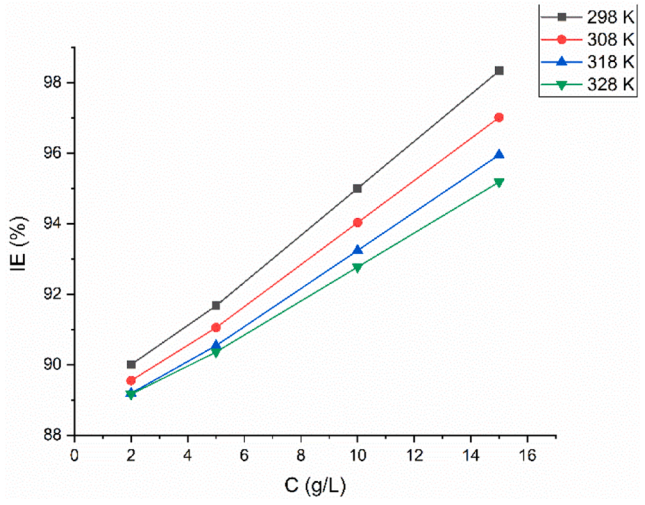

Fig. 2. The value of BLE inhibition efficiency for Cu-DHP copper corrosion in 0.5 M NaCl solution as a function of BLE concentration at different temperatures.

the following regression equations were determined:

$$y_{298} = 1.00143x + 0.352963 \quad (13)$$

$$y_{308} = 1.016643x + 0.322382 \quad (14)$$

$$y_{318} = 1.029185x + 0.297247 \quad (15)$$

$$y_{328} = 1.038943x + 0.267332 \quad (16)$$

Fig. 3 dispays the Langmuir adsorption isotherms for BLE on the copper surface Cu-DHP after 3 days in 0.5 M NaCl solution at temperatures 298 K, 308 K, 318 K, and 328 K. Based on data from Table 3 and Eq. (5), the Gibbs adsorption free energies for BLE on the copper surface solution were calculated (Table 4).

The value of ΔG_{ads}° is negative at all tested temperatures and varies in the range from –12.530 to –14.551 kJ/mol. Negative values indicate spontaneous BLE-copper adsorption and the protective film stability after adsorption [83,86]. All values are less exergonic than –20 kJ/mol, confirming the physical BLE adsorption in a 0.5 M NaCl solution across temperatures 298–328 K [30,87,88]. It is the result of electrostatic interactions among charged partners and ions from the electrolyte itself. Adsorption of negative species occurs when the metal surface is positively charged, while positively charged species can also have a protective effect on the positively charged metal by acting on negatively charged intermediates such as acid anions adsorbed on the metal surface [83]. When the chemical adsorption is absent, Coulomb forces may occur between the adsorbed cations and anions, which increases the value of ΔG_{ads}° [35] and indicates that BLE adsorption is faster with increasing temperature [86]. Since the change in the value of the adsorption constant in Table 4 is very small, this means that the adsorption of BLE molecules or complexes is not temperature-dependent.

3.4. The influence of temperature on the copper corrosion process in a 0.5 M NaCl solution

3.4.1. Activation parameters of the copper corrosion process in a 0.5 M NaCl solution

Temperature has a pronounced influence on metal dissolution, often leading to an exponential increase in corrosion rate with increasing temperature, particularly in acidic conditions [26]. Based on weight-loss measurements of copper exposed for three days to 0.5 M NaCl solutions without and with BLE (2–15 g/L) at different temperatures, the activation parameters of the corrosion process were evaluated. The temperature dependence of the corrosion rate was analyzed using Arrhenius plots (Fig. 4), which exhibited high linearity, with correlation coefficients of 0.998023 (0 g/L), 0.998707 (2 g/L), 0.998264 (5 g/L), 0.994264 (10 g/L), and 0.913331 (15 g/L). From the slopes (−Ea/R), the activation energies were determined, while the intercepts (lnA) provided the Arrhenius constants (Table 5).

Table 4
Gibbs free energy values for the adsorption of BLE on the Cu-DHP surface in a 0.5 M NaCl solution after 3 days and at different temperatures.

T (K)	K_{ads} (L/mol)	$-\Delta G_{ads}^{\circ}$ (kJ/mol)
298	2.833	12.530
308	3.102	13.184
318	3.364	13.826
328	3.741	14.551

The calculated activation energies increase in the presence of BLE and rise progressively with increasing inhibitor concentration. The higher Ea values relative to the uninhibited system indicate spontaneous adsorption of BLE molecules on the copper surface and are characteristic of a physisorption-dominated inhibition mechanism [8,9,39,83,89]. This proportional increase in activation energy reflects an enhanced energy barrier for the corrosion reaction [90], implying that the inhibitor reduces the number of available active sites on the copper surface and consequently limits the area over which corrosion can occur [34]. The observed increase in Ea can therefore be attributed to a modification of the corrosion pathway induced by the adsorption of BLE molecules and/or BLE–copper complexes, confirming their inhibitory action under chloride conditions [40]. Although BLE adsorption occurs predominantly via physical interactions, the increase in activation energy further suggests that inhibitor desorption becomes more pronounced at elevated temperatures, leading to a gradual increase in the corrosion rate as temperature rises [35,91].

The standard activation enthalpy and entropy were calculated using the equation derived from the transition state theory (Eq. (9)) [8]. The transition state diagram (Fig. 5) revealed the following correlation coefficient: 0.992338 (0 g/L), 0.998207 (2 g/L), 0.997978 (5 g/L), 0.990889 (10 g/L) and 0.903007 (15 g/L). The activation enthalpy was determined from the slope $-\Delta H^{o}/R$, while the activation enthalpy was calculated from the intercept $lnR/Nh + \Delta S^{o}/R$ (Table 5). Copper activation enthalpies are positive in a 0.5 M NaCl solution without and with BLE, indicating its endothermic nature during corrosion, meaning that

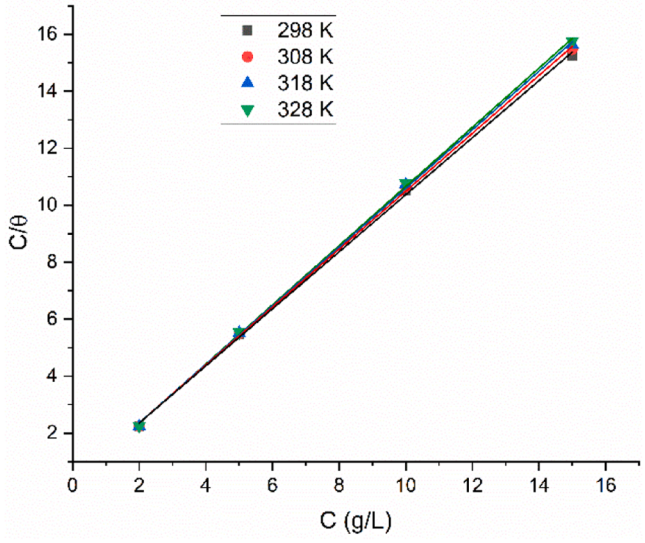

Fig. 3. Langmuir adsorption isotherms for Cu-DHP in 0.5 M NaCl solution with the addition of BLE at different electrolyte temperatures after 3 days.

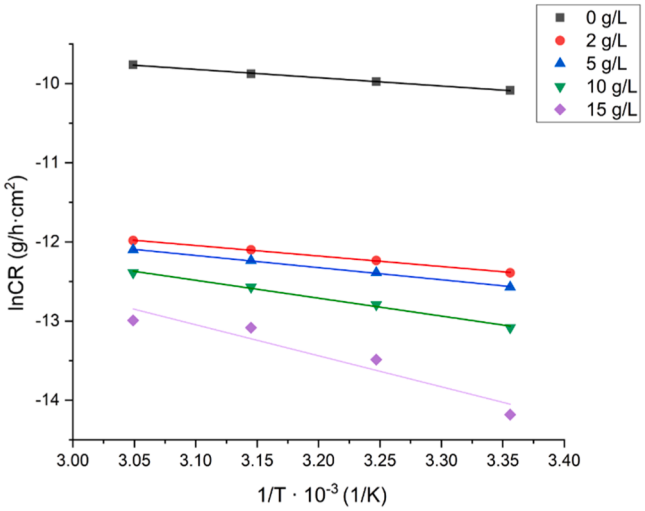

Fig. 4. Arrhenius plot for Cu-DHP in 0.5 M NaCl solution with and without BLE (2 g/L-15 g/L), after 3 days, at different temperatures (298 K-328 K).

Table 5
Calculated values of the activation parameters for Cu-DHP in 0.5 M NaCl solution with and without BLE (2 g/L-15 g/L).

C_{inh} (g/L)	Ea (kJ/mol)	ΔH^o(kJ/mol)	ΔS^o(J/mol)
0	8.720	6.086	−308
2	11.023	8.867	−318
5	12.750	10.253	−315
10	18.789	16.217	−300
15	32.574	30.107	−261

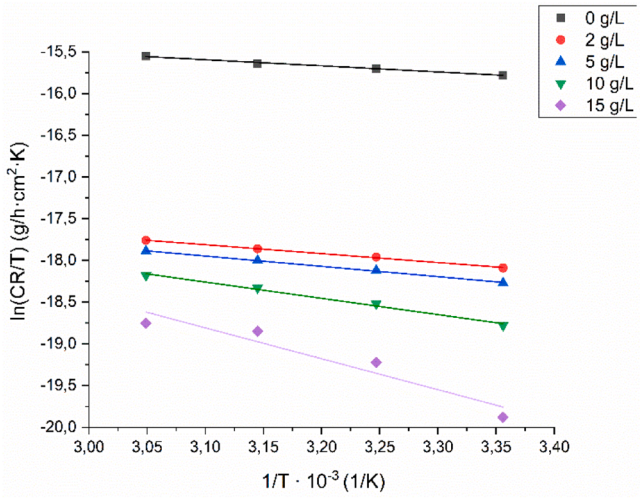

Fig. 5. Transition state diagram for Cu-DHP in 0.5 M NaCl solution without and with BLE addition (2 g/L-15 g/L), after 3 days, at different temperatures (298 K-328 K).

copper corrosion is slowed down in the presence of BLE [35,83,86]. Based on the activation enthalpies of (Table 5), BLE presence increases the activation enthalpy relative to those without BLE. This is attributed to the energy barrier of the corrosion reaction and indicates that there is an increase in the entropy of the corrosion process due to BLE adsorption [35].

A comparison of the activation entropy (ΔS^o) values in Table 5 shows that, in the presence of BLE at concentrations of 2 and 5 g/L, $\Delta S^{\ddagger}$ decreases relative to the blank solution. At 10 g/L BLE, the activation entropy is comparable to that of the uninhibited system, whereas at 15 g/L BLE, ΔS^o increases to more positive values. In the blank solution, the transition state associated with the recombination of species on the copper surface during corrosion is more ordered than the initial state, resulting in a relatively high activation entropy for the uninhibited corrosion process [35]. The decrease in ΔS^o observed at BLE concentrations below 15 g/L indicates that the formation of the activated complex is accompanied by a reduction in disorder, suggesting an associative process during inhibitor adsorption and complex formation [86,92].

More positive activation entropy values in the presence of inhibitors reflect increased disorder in the transition from reactants to the activated complex and indicate that entropy plays a significant role in determining the corrosion rate [35]. This interpretation is supported by UV–Vis spectroscopy, which revealed the presence of stable organometallic copper–BLE complexes at lower inhibitor concentrations [13]. In addition, changes in activation entropy can be correlated with a modification of the corrosion mechanism, as seen from variations in the Warburg constant obtained from electrochemical impedance spectroscopy measurements [12]. Specifically, copper corrosion in 0.5 M NaCl without BLE and in the presence of BLE concentrations below 15 g/L is predominantly controlled by activation/diffusion processes, whereas at 15 g/L BLE the corrosion process becomes governed by charge-transfer kinetics [93]. Under charge-transfer control, increased disorder is associated with the formation of a less stable and sparsely populated activation complex due to the reduced availability of copper ions in solution. In contrast, when corrosion is controlled by activation/diffusion, the system is more ordered, either due to the formation of stable organometallic complexes or because the copper surface is sufficiently covered by BLE molecules, thereby limiting disorder during the corrosion process.

3.4.2. Thermodynamic parameters of the copper corrosion process in 0.5 M NaCl solution

The thermodynamic parameters were calculated using the Van Hoff Eq. (6), the Gibbs-Helmholtz Eq. (7) and the basic equation of thermodynamics (8). Using the values from Table 4, the thermodynamic parameters were calculated and presented in Table 6. For each thermodynamic equation, large values for the correlation coefficient were obtained: 0.994395 (Van Hoff equation), 0.995427 (Gibbs-Helmholtz equation) and 0.999239 (basic equation of thermodynamics).

Data in Table 6 show that similar values of adsorption enthalpy and adsorption entropy were obtained by applying different thermodynamic equations. The positive value of adsorption enthalpy ΔH^o_{ads} indicates that the adsorption process of BLE molecules and BLE-copper complexes is an endothermic process [32]. Values less than 40 kJ/mol confirm that the physical adsorption of BLE on the copper surface occurs in a 0.5 M NaCl solution [35,94]. The change in adsorption entropy ΔS^o_{ads} is positive, indicating that when BLE is adsorbed onto the copper surface, system disorder is created, being the driving force for the inhibitor adsorption [86,92,95]. The reason for the positive value of adsorption entropy may be the desorption of water molecules from the copper surface during the adsorption of BLE molecules or organometallic complexes, which increases the entropy of the solvent [96].

3.5. Response surface methodology (RSM) and optimization of the corrosion inhibition process

The results of the RSM used to determine the synergistic effect of copper immersion time in the electrolyte, temperature and BLE concentration on the copper corrosion inhibition process were performed using the data from Table 7. The statistical significance of the individual variables and the CCD model was determined using analysis of variance (ANOVA). The values of the independent and dependent variables used for RSM by the CCD model, the number of random experiments (std. order) and the actual order (run order) of the experiments performed are shown in Table 7. The independent variables are the immersion time of the copper in the electrolyte (time, h), the temperature (K) and the concentration of the inhibitor (Cinh, g/L). After forming the CCD model and performing the experiments, the values of corrosion rate (CR, μg/h·cm^2) and inhibition efficiency (IE, %) were used to complete the CCD model. An RSM was performed for each dependent variable. Normality plots and residual distribution plots with respect to the fitted values, linear, quadratic and 2-way interaction analysis with a confidence level of 0.05, analysis of variance and statistical model were obtained as RSM results. Contour and 3D plots were created based on the statistically significant variables (corrosion rate and inhibition efficiency).

The statistical parameters of the CCD model are summarized in Table 8. The high adjusted coefficients of determination (R^2(adj)) show the model accurately predicts both the corrosion rate and inhibition

Table 6
Adsorption properties of BLE when adsorbed on a copper surface in a 0.5 M NaCl solution.

Thermodynamic equation	ΔH^o_{ads} (J/mol)	ΔS^o_{ads}(J/mol·K)
Van Hoff	7422	66.92
Gibbs–Helmholtz equation	7710	-
Basic equation of thermodynamics	7464	67.05

Table 7
CCD design for the Cu-DHP corrosion inhibition process in 0.5 M NaCl using BLE.

Std. order	Run order	Time (h)	Temperature (K)	C_{inh} (g/L)	CR (μg/h·cm^2)	IE (%)
20	1	156.000	315.500	10.000	2.980	94.33
17	2	156.000	315.500	10.000	2.980	94.33
3	3	72.000	328.000	5.000	5.560	90.36
6	4	240.000	303.000	15.000	0.477	98.90
12	5	156.000	336.522	10.000	3.360	93.30
2	6	240.000	303.000	5.000	0.893	97.90
7	7	72.000	328.000	15.000	2.280	95.18
10	8	297.271	315.500	10.000	0.105	96.02
18	9	156.000	315.500	10.000	3.030	94.30
15	10	156.000	315.500	10.000	3.080	94.29
4	11	240.000	328.000	5.000	3.460	94.20
1	12	72.000	303.000	5.000	3.850	91.33
14	13	156.000	315.500	18.409	1.080	96.12
5	14	72.000	303.000	15.000	1.050	97.71
19	15	156.000	315.500	10.000	2.960	94.35
13	16	156.000	315.500	1.591	4.560	88.89
9	17	14.729	315.500	10.000	3.170	93.74
11	18	156.000	294.478	10.000	1.190	96.30
8	19	240.000	328.000	15.000	1.180	97.10
16	20	156.000	315.500	10.000	3.360	93.30

Table 8
Model parameters.

	R^2%	R^2 (adj)%	R^2 (pred)%
Corrosion rate	98.71	97.55	91.03
Inhibition efficiency	98.70	97.52	90.97

efficiency [97]. Likewise, the R^2 values demonstrate the high accuracy of the developed models [98]. In general, a model is considered satisfactory when $R^2 \geq 0.8$ [99], and the R^2 values obtained for the CCD model in Table 8 significantly exceed this threshold, confirming excellent agreement between experimental data and model predictions [100]. Ideally, R^2 should approach unity, reflecting minimal unexplained variance. Furthermore, acceptable agreement between R^2 and R^2(adj) is typically achieved when their difference is less than 0.2 (20%) [21]. The close similarity between these parameters for both response models confirms their high statistical significance and robustness [46,97,98]. The predictive coefficient of determination (R^2(pred)) provides additional insight into the predictive capability of the model and indicates whether excessive, non-influential terms have been included. Large deviations between R^2 and R^2(pred) suggest overfitting, which adversely affects predictive reliability, for example, an R^2 of 87% combined with an R^2(pred) of 52% [101]. In the present study, the R^2(pred) values do not deviate substantially from the corresponding R^2 values, indicating that the models are not overfitted and contain no significant amount of redundant data. The strong correlation between predicted and experimental values further confirms the adequacy of the CCD models, which can therefore be reliably used to predict copper corrosion rates and inhibition efficiencies in 0.5 M NaCl as a function of BLE concentration, temperature, and copper immersion time [46].

Additional confirmation of the adequacy of the model was determined by normal probability plots for the variable corrosion rate (Fig. 6a) and the variable inhibition effect (Fig. 6b). Both plots confirm the normality of the sample distribution, which also confirms variance constancy [46,97].

The plots of residuals versus fitted values for the corrosion rate and inhibition efficiency are presented in Fig. 7a and 7b, respectively. Residuals, defined as the differences between experimentally measured and model-predicted values for a given set of conditions, are used to assess the adequacy of the fitted model [102]. Analysis of residual distributions allows verification of the assumptions of random error distribution and constant variance. Ideally, residuals should be randomly scattered around zero without any discernible patterns [101]. As shown in Fig. 7a and 7b, the residuals for both corrosion rate and inhibition efficiency are randomly distributed about zero, confirming the validity and reliability of the developed CCD models for Cu-DHP corrosion inhibition by BLE in 0.5 M NaCl.

Table 9 presents the analysis of variance (ANOVA) results for the CCD model describing the corrosion rate. Based on the model analysis and ANOVA outcomes, a regression equation for the corrosion rate was derived using uncoded (actual) values:

$$CR\left(\mu g/h{\cdot}cm^2\right) = -182.4 - 0.0119\ Time(h) + 1.099\ Temperature(K) + 1.152\,C_{inh}(g/L) - 0.000067\ Time\,(h){\cdot}Time(h) - 0.001586\ Temperature(K){\cdot}Temperature(K) - 0.00220\ C_{inh}(g/L){\cdot}C_{inh}(g/L) + 0.000039\ Time(h){\cdot}Temperature(K) + 0.001007\ Time(h){\cdot}C_{inh}(g/L) - 0.00469\ Temperature(K){\cdot}C_{inh}(g/L) \quad (17)$$

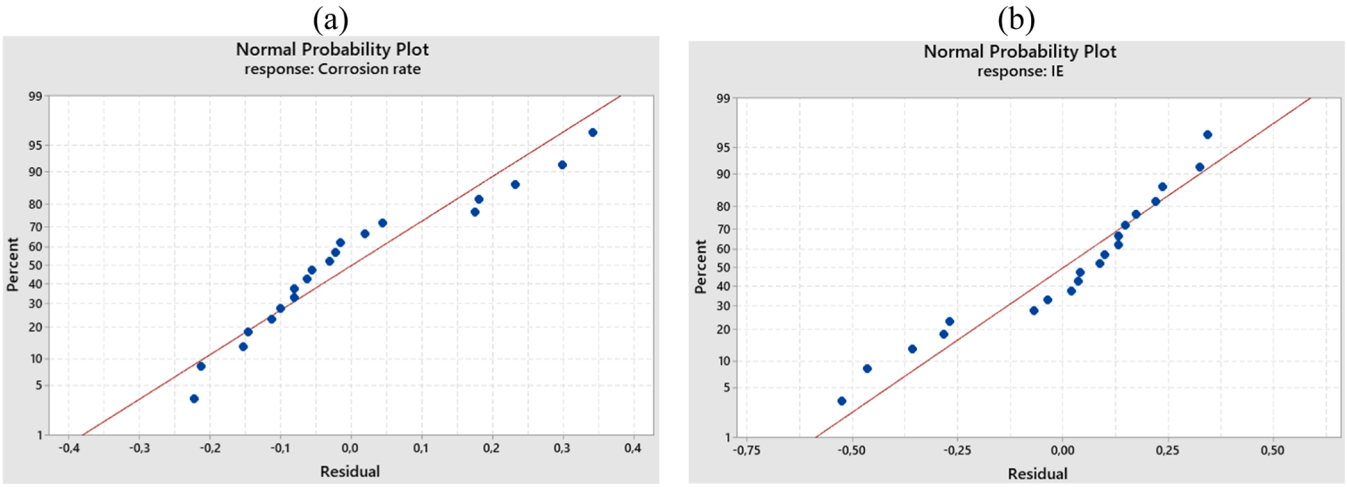

Fig. 6. Normal probability plots for the values of a) corrosion rate and b) inhibition efficiency.

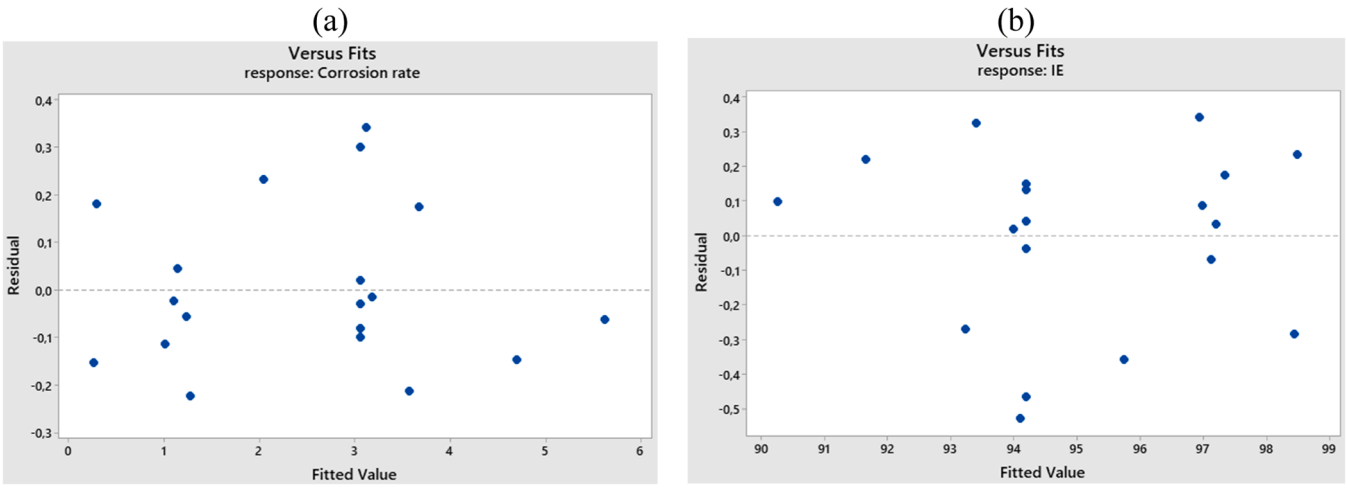

Fig. 7. Plots of residuals versus fitted values for a) corrosion rate and b) corrosion inhibition efficiency of Cu-DHP by BLE in 0.5 M NaCl solution.

Table 9
Analysis of variance (ANOVA) of the CCD model for the corrosion rate.

	DF	Adj SS	Adj MS	F-value	P-value
Model	9	39.0769	4.3419	85.01	0.000
Linear	3	33.1301	11.0434	216.23	0.000
Time (h)	1	10.3425	10.3425	202.51	0.000
Temperature (K)	1	7.1180	7.1180	139.37	0.000
C_{inh} (g/L)	1	15.6696	15.6696	306.81	0.000
Square	3	3.8150	1.2717	24.90	0.000
Time (h)· Time (h)	1	3.2266	3.2266	63.18	0.000
Temperature (K)·Temperature (K)	1	0.8848	0.8848	17.32	0.002
C_{inh} (g/L)·C_{inh} (g/L)	1	0.0438	0.0438	0.86	0.376
2-Way interaction	3	2.1318	0.7106	13.91	0.001
Time (h)·Temperature (K)	1	0.0136	0.0136	0.27	0.617
Time (h)·C_{inh} (g/L)	1	1.4314	1.4314	28.03	0.000
Temperature (K)·C_{inh} (g/L)	1	0.6868	0.6868	13.45	0.004
Error	10	0.5107	0.0511		
Lack of fit	5	0.3968	0.0794	3.48	0.099
Error	5	0.1139	0.0228		
Total	19	39.5876			

All necessary data for a complete CCD model analysis were provided by the ANOVA regression. The DF data indicates the number of degrees of freedom for all model data. The information is used to predict the unknown values in the population. The number of sample observations determines the total number of DF. It indicates how much information each part of the model contains. Increasing the sample size provides more information about the population and therefore increases the total DF. When more terms are specified in the model, the DF available for assessing the variable parameters needed for prediction decreases as less information is available [103]. The Adj SS and Adj MS values are the adjusted sum of squares and the adjusted mean square value, respectively. The value of Adj SS indicates the measurement variation of the different constituent models, while Adj MS shown the variation of a term or model based on all other terms that the model contains, regardless of their order of occurrence. Unlike Adj SS, Adj MS contains the number of degrees of freedom [103,104]. Based on the significance level p and the p-value of the CCD model for analyzing the influence of the immersion time of copper in a 0.5 M NaCl solution with the addition of BLE, temperature and inhibitor concentration, the model was found to be statistically significant ($p \leq 0.05$) [21,97]. All three investigated factors have a statistically significant influence on the copper corrosion rate. The F-value is a statistical test that checks whether the investigated phase is related to the reaction [103,104]. The F-test value can be used to determine which factor has the greatest influence on the corrosion rate [24,97]. The highest value of the F-test (306.81) was obtained for

Table 10
Analysis of variance (ANOVA) of the CCD model for inhibition efficiency.

	DF	Adj SS	Adj MS	F-value	P-value
Model	9	92.3260	10.2584	84.18	0.000
Linear	3	78.3123	26.1041	214.20	0.000
Time (h)	1	24.4458	24.4458	200.59	0.000
Temperature (K)	1	16.8193	16.8193	138.01	0.000
C_{inh} (g/L)	1	37.0472	37.0472	303.99	0.000
Square	3	8.9951	2.9984	24.60	0.000
Time (h)· Time (h)	1	7.6119	7.6119	62.46	0.000
Temperature(K)·Temperature (K)	1	2.0809	2.0809	17.08	0.002
C_{inh} (g/L)·C_{inh} (g/L)	1	0.1006	0.1006	0.83	0.385
2-Way interaction	3	5.0186	1.6729	13.73	0.001
Time (h)·Temperature (K)	1	0.0339	0.0339	0.28	0.609
Time (h)·C_{inh} (g/L)	1	3.3710	3.3710	27.66	0.000
Temperature (K)·C_{inh} (g/L)	1	1.6137	1.6137	13.24	0.005
Error	10	1.2187	0.1219		
Lack of fit	5	0.9414	0.1883	3.40	0.103
Error	5	0.2773	0.0555		
Total	19	93.5447			

the independent variable C_{inh}, indicating that the BLE concentration has the greatest influence on the copper corrosion rate. The immersion time has a lower influence (202.51), followed by the temperature (139.37). Of the square factors, immersion time ($p = 0.000$) and temperature ($p = 0.002$) have a statistically significant influence. Immersion time and inhibitor concentration ($p = 0.000$) and temperature and inhibitor concentration ($p = 0.004$) are the two-way interactions that have a statistically significant influence. The value for the lack of fit describes the changes in the data around the fitted model. If the results show that this parameter is statistically significant, it means that the model is not well fitted [105]. Since the value of the lack of fit ($p = 0.099$) in Table 9 is greater than 0.05 for the fitted second order model in terms of corrosion rate, it means that the adequate fit of the model is confirmed.

Table 10 shows the ANOVA results for the CCD model of the inhibition efficiency, leading to a regression equation for inhibition efficiency was established using the uncoded values:

$$\begin{aligned} IE\,(\%) = {} & 378.6 + 0.0188\ Time\ (h) - 1.686\ Temperature\ (K) - 1.763\ C_{inh}(g/L) + 0.000103 \\ & Time\ (h)\cdot Time\ (h) + 0.002432\ Temperature\ (K)\cdot Temperature\ (K) + 0.00334\ C_{inh}(g/L)\cdot C_{inh}(g/L) - \\ & 0.000062\ Time\ (h)\cdot Temperature\ (K) - 0.001546\ Time\ (h)\cdot C_{inh}(g/L) + \\ & 0.00719\ Temperature\ (K)\cdot C_{inh}(g/L) \end{aligned} \tag{18}$$

Tables 9 and 10 reveal the same DF value for the corrosion rate, as the same CCD model was used. The part of the model related to inhibition efficiency is statistically significant as its p-value is below the statistical significance level [21,97]. Within the ANOVA analysis of the linear influence of parameters on inhibitor efficiency, all three independent variables (time, temperature and inhibitor concentration) were found to have a statistically significant influence on corrosion inhibition efficiency with BLE. Cinh ($F = 303.99$) has the greatest influence on the inhibition efficiency, followed by the immersion time of the copper in the electrolyte ($F = 200.59$) and temperature ($F = 138.01$), which has the least influence [24,97]. When analyzing the square effect of the tested parameters on the corrosion inhibition efficiency using BLE, the time ($p = 0.000$) and temperature ($p = 0.002$) have a statistically significant effect. The immersion time of copper in the electrolyte and inhibitor concentration ($p = 0.000$) and temperature ($p = 0.005$) have a statistically significant effect on inhibition efficiency when they are changed simultaneously [46,97]. The model fit regarding corrosion inhibition efficiency is adequate due to the large lack of its fit value ($p = 0.103 > 0.05$) [105]. The results of the linear, square and two-way interaction of the CCD model of corrosion rate and inhibition efficiency are statistically significant.

Figs. 8–11 present contour and surface plots illustrating the simultaneous influence of the variables whose statistical significance was identified by the CCD model. The surface (Fig. 8a) and contour (Fig. 8b) plots of the copper corrosion rate in 0.5 M NaCl solution, as a function of inhibitor concentration and immersion time, indicate that BLE is most effective as a copper corrosion inhibitor at higher inhibitor concentrations and longer immersion times. Since the change in copper corrosion rate under these conditions is not linear, due to the simultaneous change in two parameters, it is possible to determine in which areas of the contour plot BLE works best using legend for the corrosion rate value, being blue areas. This area begins when the BLE concentration in the electrolyte is slightly higher than 10 g/L, i.e. at the minimum immersion time of copper in the electrolyte. A similar change in the corrosion rate occurs at the minimum BLE concentration (about 2 g/L) when the immersion time is longer than 225 h. The corrosion rate value is lowest at all immersion times when the inhibitor concentration is greater than 12 g/L.

The simultaneous influence of the change in inhibitor concentration and temperature on copper corrosion in a 0.5 M NaCl solution is shown in the surface (Fig. 9a) and contour (Fig. 9b) diagrams. These plots clearly show the areas of inhibitor concentration and temperature where BLE works best as a corrosion inhibitor, i.e. where the copper corrosion process is slowest. These areas are shown in blue on the contour diagram and include areas with high inhibitor concentrations and low temperatures. A significant reduction in the rate of copper corrosion in a chloride environment is achieved at low temperatures (room temperature) with a BLE concentration of approximately 2 g/L. Up to about 302 K, a blue area is observed at the lowest values of BLE concentration. At higher temperatures, the corrosion rate increases, but is low at all temperatures

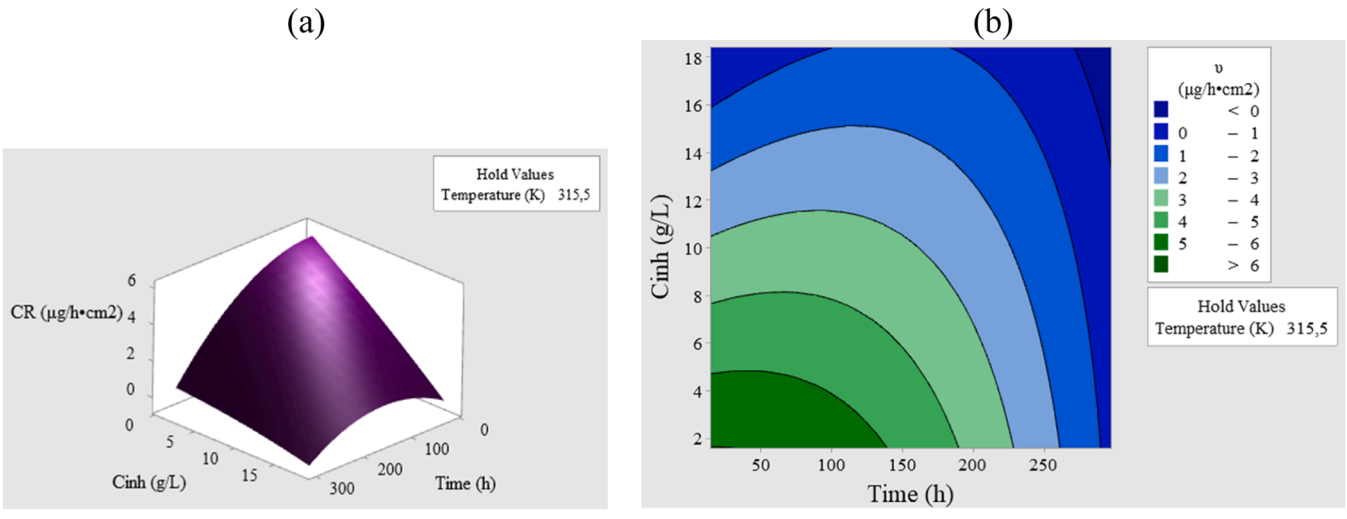

Fig. 8. Surface and contour plots of the corrosion rate of Cu-DHP in 0.5 M NaCl solution when the BLE inhibitor concentration (Cinh, g/L) and the immersion time of the copper in the electrolyte (Time, h) are changed.

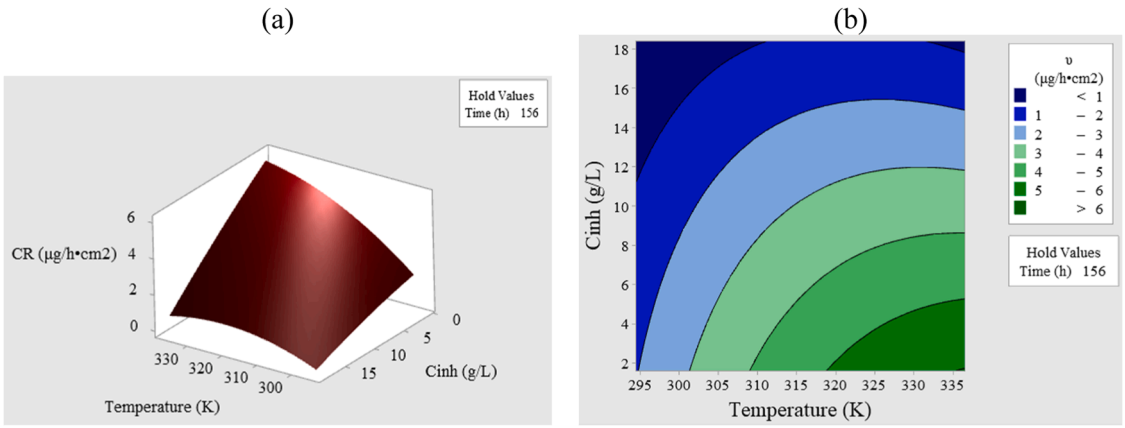

Fig. 9. Surface and contour plots of the corrosion rate of Cu-DHP in 0.5 M NaCl solution with changing concentration of BLE inhibitor (Cinh, g/L) and temperature (Temperature, K).

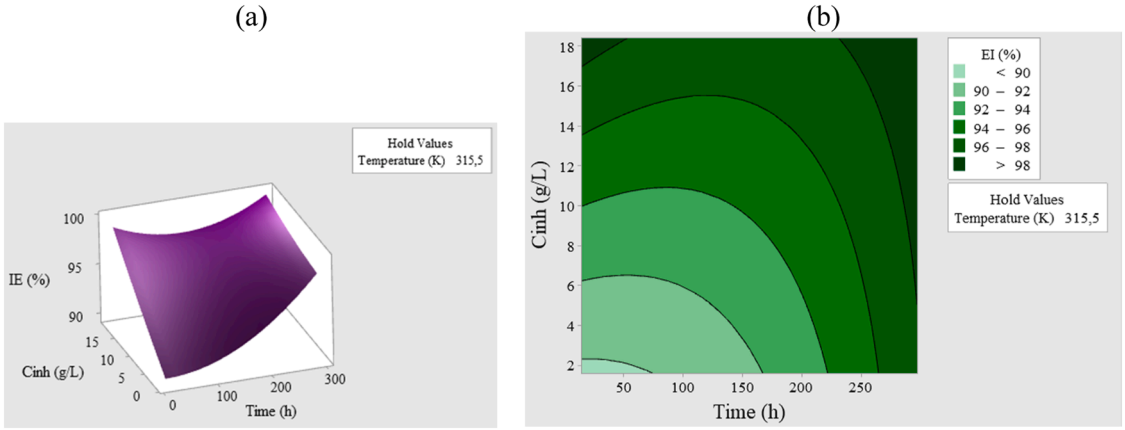

Fig. 10. Surface and contour plots of Cu-DHP corrosion inhibition efficiencyin 0.5 M NaCl solution when changing the BLE inhibitor concentration (Cinh, g/L) and the immersion time of copper in the electrolyte (Time, h).

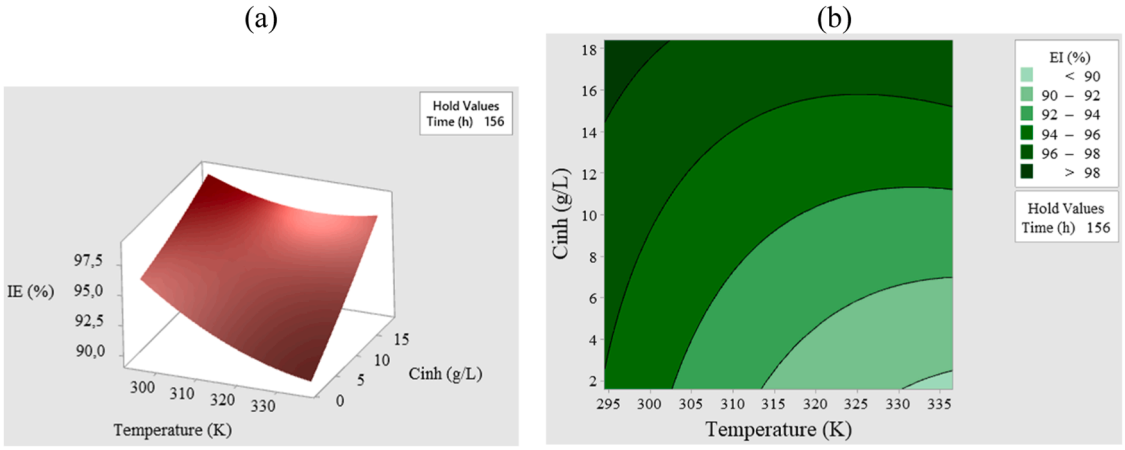

Fig. 11. Surface and contour plots of corrosion inhibition efficiency of Cu-DHP in 0.5 M NaCl solution with changing BLE inhibitor concentration (Cinh, g/L) and temperature (Temperature, K).

when the BLE concentration is above 12 g/L.

As with the copper corrosion rate, a statistically significant effect on the inhibitor efficiency is the simultaneous effect of the copper immersion time and the inhibitor concentration. The surface plot and contour surface plot are shown in Fig. 10a, 10b. The best copper inhibitor efficiency with BLE is achieved with a longer immersion time and higher BLE concentrations. The areas with the highest percentage BLE corrosion inhibition efficiency in, when the inhibitor concentration and the immersion time of copper in the electrolyte are changed simultaneously, are shown in dark green shades on the contour plot. Based on earlier literature reports, BLE acts as a very effective copper corrosion inhibitor in a chloride environment at all concentrations above 2 g/L and at a

Table 11
Prediction of the multiple reactions of the copper corrosion model in 0.5 M NaCl solution with BLE for a 99% inhibition efficiency.

Variable	Setting			
Time (h)	14.7294			
Temperature (K)	334.5640			
Cinh (g/L)	17.9282			
Response	Fit	SE Fit	95% CI	95% PI
EI (%)	99.000	0.693	(97.457; 100.543)	(97.272; 100.728)

copper immersion time of more than 70 h. Similar results were obtained for jojoba fruit peel extract, where a copper corrosion inhibition efficiency of 90% was achieved when 2 g/L jojoba peel extract was added to a 1 M HCl solution [8]. The increasing efficiency of the inhibitor over time can be explained by the fact that the metal surface becomes more covered with the inhibitor over time, forming a protective film [100]. In addition, the immersion time and BLE concentration have a synergistic effect on copper corrosion protection in 0.5 M NaCl, so that a high degree of inhibition is easily achieved [24].

Another statistically significant effect on the copper corrosion inhibition efficiency is the simultaneous effect of inhibitor concentration and temperature (Fig. 11a, 11b). The best inhibition efficiency is achieved at higher BLE concentrations and lower temperatures. The decrease in inhibitor efficiency is due to the decrease in adsorption of organic components at higher electrolyte temperatures [84,106]. This change indicates that the inhibitor undergoes physical adsorption on the metal surface [84]. The decrease in inhibition efficiency with increasing temperature can be attributed to the increase in kinetic energy, which promotes intermolecular interactions of adsorbate and adsorbent, as well as fragmentation and/or rearrangement catalyzed at high temperatures [84,88,97]. At higher BLE concentrations, a semi-elliptical shape of the contour line is observed that can be explained by a larger temperature influence on the adsorption-desorption equilibrium of the corrosion processes on the copper surface [24].

Although the plots for the change in corrosion rate and inhibition efficiency with BLE show the same effect of temperature, copper immersion time and inhibitor concentration, there is a discrepancy between them. It arises because the value determined on the basis of three experiments, performed simultaneously on a copper plate under the same conditions, is used to form the corrosion rate model. For the inhibition efficiency model, the calculated values representing the masses of three copper coupons treated under the same conditions with BLE at the concentration specified by the model and three copper coupons tested under the same conditions of immersion time and temperature as the previous ones but without the addition of inhibitor were used. By exposing three copper coupons to the same conditions at the same time, the possibility of random error is minimized, as is the difference between the models. Common to all diagrams is that BLE performs best at concentrations exceeding 12 g/L, where there is a change in the adsorption mechanism on the copper surface, as determined by the EIS method, with a change from diffusion-controlled corrosion processes to a process that depends on charge transfer [12].

Based on the results of the CCD model (Table 7), the BLE exhibits the highest inhibition efficiency percentage (98.90%) at 303 K, an immersion time of 240 h and an inhibitor concentration of 15 g/L. In addition to the value of the model and the its parameters, it is possible to predict the corrosion inhibition efficiency value and determine under which conditions this value is achieved [104]. For example, optimizing the model to achieve the corrosion inhibition of 99% yields the predicted values for the multiple response shown in Table 11 and Fig. 12. The 95% CI is the confidence interval and the 95% PI is the predicted interval [107,108]. This means that there is a 95% probability of achieving an inhibition efficiency of 99%, with a confidence interval of 97.457% to 100.543% and a predicted interval of 97.272% to 100.728%, for a copper immersion time of 14.7294 h in an electrolyte containing 0.5 M NaCl with the addition of 17.9282 g/L BLE, at 334.5640 K. It should be considered that the model provides values that are outside the real values. Thus, if the optimization of the maximum efficiency of the inhibitor or the minimum value of the corrosion rate is performed, the model may show values above 100% for the inhibition efficiency and negative values for the corrosion rate. In this way, it is up to the researcher to decide which threshold values to consider.

In order to reduce the shortcomings to a minimum, the optimization of the corrosion inhibition of Cu-DHP in 0.5 M NaCl with a fixed value of the corrosion inhibitor concentration (15 g/L BLE) is given as a further example when the inhibition efficiency is 99%. The optimization results are shown in Table 12 and Fig. 13. A temperature of 294.478 K and a copper immersion time of 213.466 h are required to achieve an inhibitor efficiency of 99% when 15 g/L BLE is added. Multiple response analysis on the prediction determined the confidence interval of inhibition efficiency using BLE from 98.122% to 99.878%, with a confidence of 95% and the predicted interval from 97.827% to 100.173%. For a more complete verification of the model and the statistical data allowing the prediction of the variables, the indicated parameters were applied experimentally using the weight loss method. As a result of the analysis, a value of 99.05% inhibitor efficiency was obtained. The value obtained is within the confidence interval and the predicted interval, which

Table 12
Prediction of the multiple responses of the copper corrosion model in 0.5 M NaCl solution with 15 g/L BLE for 99% inhibition efficiency.

Variable	Setting			
Time (h)	213.466			
Temperature (K)	294.478			
Cinh (g/L)	15			
Response	Fit	SE Fit	95% CI	95% PI
EI (%)	99.000	0.394	(98.122; 99.878)	(97.827; 100.173)

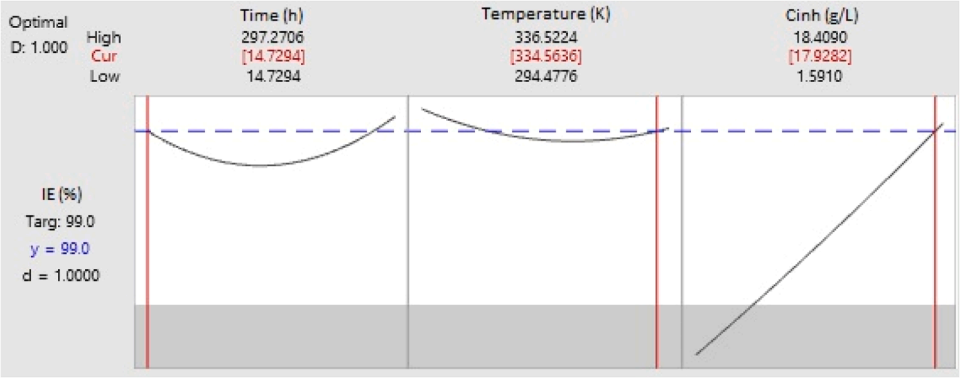

Fig. 12. Optimization parameters of Cu-DHP copper corrosion inhibition in 0.5 M NaCl solution with the addition of BLE when the inhibition efficiency is 99%.

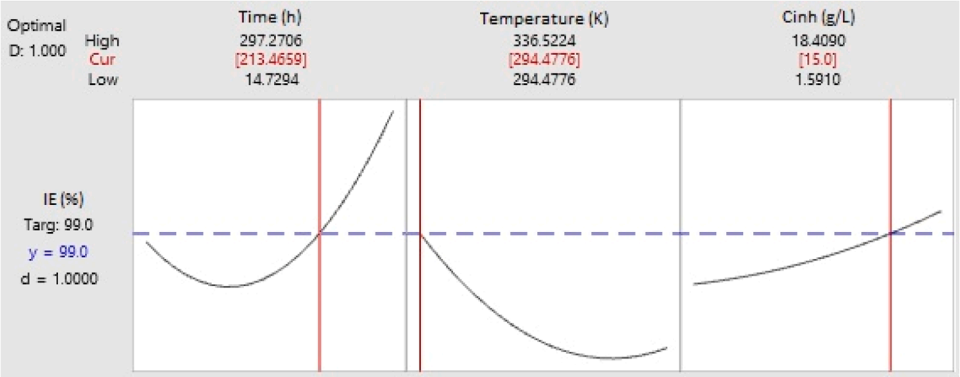

Fig. 13. Optimization parameters of Cu-DHP copper corrosion inhibition in a solution 0.5 M NaCl with the addition of 15 g/L BLE when the inhibition efficiency is 99%.

confirms that with an adequate optimization of the corrosion process a better inhibitor efficiency can be obtained than with classical experiments with only one factor considered. Comparing the value obtained with the value for the inhibition efficiency value of 99.1% obtained at a temperature of 295 K and an immersion time of 240 h, it is clear that the immersion time influenced the increase in the inhibition efficiency value. However, the potential long-term performance and stability of BLE as an inhibitor are unknown, which could be further investigated in the future.

3.6. Mechanism of BLE adsorption on the copper surface in 0.5 M NaCl solution

The adsorption of the inhibitor depends on its chemical structure, the size of the molecule, the nature and charge of the metal surface and the charge distribution throughout the inhibitor molecule. In fact, the adsorption process can occur by the replacement of solvent molecules from the metal surface by ions and molecules that accumulate near the metal/solution interface. More ions can accumulate at the metal/solution interface than are required to balance the charge of the metal at equilibrium potential. These ions displace the solvent molecules from the copper surface and their centers are located in the inner Helmholtz plane. This phenomenon is called specific adsorption or contact adsorption [109]. Anions are adsorbed when the metal surface has an excess of positive charge greater than that required to balance the charge corresponding to the applied potential. The exact nature of the interaction between the alloy surface and the aromatic molecule depends on the relative coordination strength of the functional groups present to the metal in question [110].

Based on the results and the literature reviewed, the BLE adsorption mechanism on the copper surface in a 0.5 M NaCl solution can be assumed. BLE acts as a corrosion inhibitor by physically adsorbing molecules and organometallic complexes on the copper surface according to the Langmire adsorption isotherm. At BLE concentrations lower than 10 g/L, organometallic complexes of copper ions formed by copper corrosion and inhibitor molecules are produced. Literature assumes that all three BLE components can form stable complexes with Cu (II) ions [9,11]. Earlier, caffeic acid was shown to be a cathodic copper corrosion inhibitor in a 0.5 M NaCl solution by adsorbing to the copper surface via a non-covalent bond, with the entire surface directed towards the copper surface [111]. Since plant extracts have several heteroatoms in compounds, synergistic effects between the molecules can occur, resulting in a good inhibition efficiency [109]. BLE acts as a mixed type of corrosion inhibitor, so it is clear that in addition to caffeic acid, quercetin-3-O-glucoside and kaempferol-3-O-glucoside also influence the same processes. The inhibitory effect of BLE on copper corrosion can be rationalized based on the activation and adsorption parameters. The BLE adsorption on the copper surface reduces the corrosive effect of the electrolyte, whereby BLE molecules can replace previously adsorbed water molecules [112]. At lower BLE concentrations, the system is better organized due to the association of the molecules and the reduction of corrosion products. As with copper corrosion in 0.5 M NaCl solution without BLE, the corrosion mechanism is activated/diffusion-controlled at BLE concentrations of less than 10 g/L.

Most often, water-inhibitor substitution is considered as the first step of corrosion inhibition [113]:

$$inh_{(sol)} + nH_2O_{(ads)} \rightarrow inh_{(ads)} + nH_2O \quad (19)$$

where n is the number of water molecules that can be replaced by inhibitor molecules.

In addition to the synergistic effect of the BLE molecules, it should be noted that the ions of the halogen elements have a positive effect on the inhibition of the corrosion process by organic inhibitors. Thus, the presence of chloride ions in the 0.5 M NaCl solution does not have a corrosive effect, but promotes the effect of BLE as a corrosion inhibitor. According to the first mechanism, ion pairs are formed in the bulk of the solution and then adsorbed from the solution to the metal surface as follows [61]:

$$Y_s + X_s \rightarrow (YX)_s \quad (20)$$

$$(YX)_s \rightarrow (YX)_{ads} \quad (21)$$

The second mechanism states that first the halide ion is adsorbed on the metal surface, whereupon the inhibitor molecule is attracted to the double layer by the adsorbed halide ion, so that ion pair formation occurs directly on the metal surface. The second mechanism can be shown as follows [61]:

$$X_s \rightarrow X_{ads}\, Y_s + X_{ads} \rightarrow (YX)_{ads} \quad (22)$$

where Y_s is the inhibitor molecule, X_s is the halide ion, $(YX)_s$ is the ion pair in the bulk solution, Y_{ads}, X_{ads} and $(YX)_{ads}$ are the adsorbed species [61–63].

The adsorption of caffeic acid, quercetin-3-O-glucoside, kaempferol-3-O-glucoside, their organometallic complexes and ion pairs on forms a protective film. Its formation prevents the corrosion, whereas the inhibitor influences the formation reactions of CuCl and $CuCl_2^-$, as well as Cu_2O and $Cu_2(OH)_3Cl$ [114]. The surface coverage of organic molecules depends on their metal surface orientation. The planary orientation of the inhibitor molecules in relation to the metal surface covers a larger area, so that better protection against corrosion can be expected – a more optimal inhibition is achieved in this way than involving a vertical orientation. By using simulation methods, it is possible to determine which part of the molecule interacts with the metal surface [97].

As the BLE concentration increases, more inhibitor species are available for the copper surface adsorption, increasing the surface

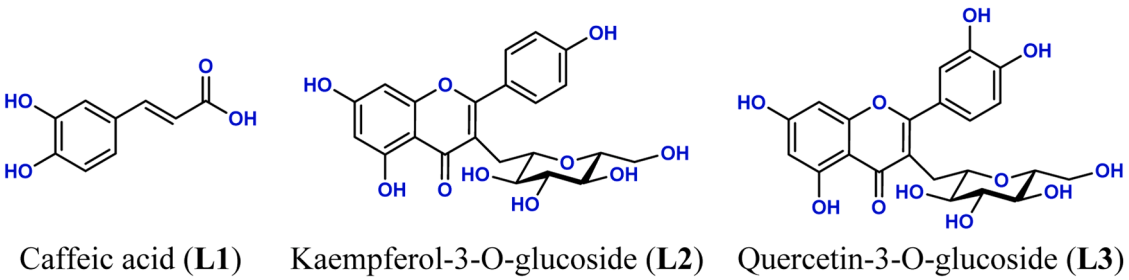

Fig. 14. Chemical structure of investigated ligands.

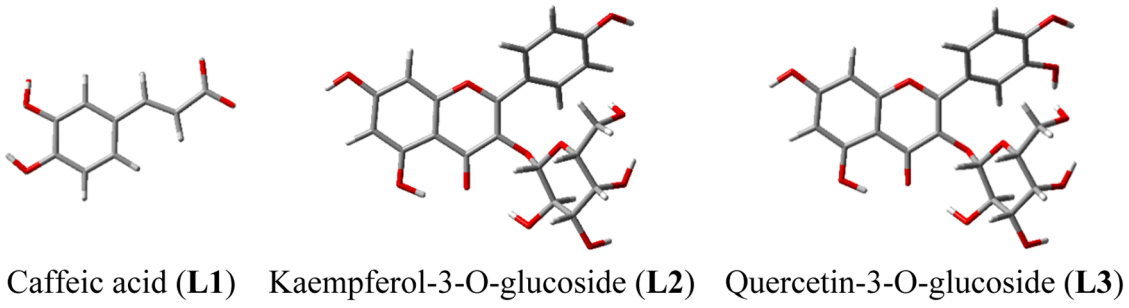

Fig. 15. The most stable geometries of investigated ligands as obtained wth the (SMD)/M06–2X/def2-TZVP model in water.

coverage, decreasing the corrosion rate, and increasing the corrosion inhibition efficiency. When the surface coverage is sufficient, there are not enough copper ions to form an organometallic complex, so the presence of the complex was not detected at higher BLE concentrations [13]. However, at BLE concentrations exceeding 10 g/L, there is a change in the mechanism [12]. Disorder then occurs in the transition from the reactant to the activated complex to a degree that determines the reaction rate. With 15 g/L BLE, unstable complexes are formed, which could be the result of a mechanistic change. In addition, much less copper chloride is present and no copper oxide is formed when the BLE concentration is 15 g/L [11]. The corrosion process accelerates with increasing temperature, even when BLE is present. The decrease in the corrosion inhibition effectiveness with BLE at higher temperatures indicates that there is a physical adsorption of inhibitor molecules on the copper surface [84]. Higher temperatures offer incerased kinetic energies, leading to catalyzed fragmentation and/or rearrangement [97]. As the copper is immersed in the electrolyte, the efficiency of BLE increases as a greater copper surface area is covered with the inhibitor over time [100]. BLE works best as a copper corrosion inhibitor in a chloride-containing environment at lower temperatures, with prolonged immersion of the copper in the electrolyte and at higher concentrations of BLE.

3.7. Computational DFT analysis

Computational analysis was employed to identify organometallic complexes in solution and aid in interpreting experimental observations. The feasibility of complex formation between Cu(II) ions and three organic ligands – caffeic acid (**L1**), kaempferol-3-O-glucoside (**L2**), and quercetin-3-O-glucoside (**L3**) was investigated, focusing on their stoichiometry and thermodynamic stability (Fig. 14).

L2 and **L3** are structurally similar, differing only by an additional –OH group on the phenyl ring in the latter, suggesting comparable Cu(II) complexation behavior. Literature indicates phenol deprotonation typically occurs at pH ≈ 10, which is beyond experimental conditions in this case. Although the extra –OH group in **L3** slightly increases phenol acidity (pK_a = 9.99 for 4-phenol, 9.40 for 3,4-dihydroxy) [115], the required pH still exceeds our experimental range, rendering –OH deprotonation irrelevant for our analysis. Aliphatic alcohols, less acidic than phenols, further support the predominance of neutral, unionized forms of **L2** and **L3** in solution, as modeled. Conversely, caffeic acid (**L1**), a weak organic acid with a pK_a of 4.62, was considered mono-deprotonated at the carboxylic group ($–COO^-$).

The first step was analyzing the stability of isolated ligands **L1**–**L3**, with the most stable conformations shown in Fig. 15. Caffeic acid (**L1**) exhibits intramolecular O–H···O hydrogen bonding between adjacent

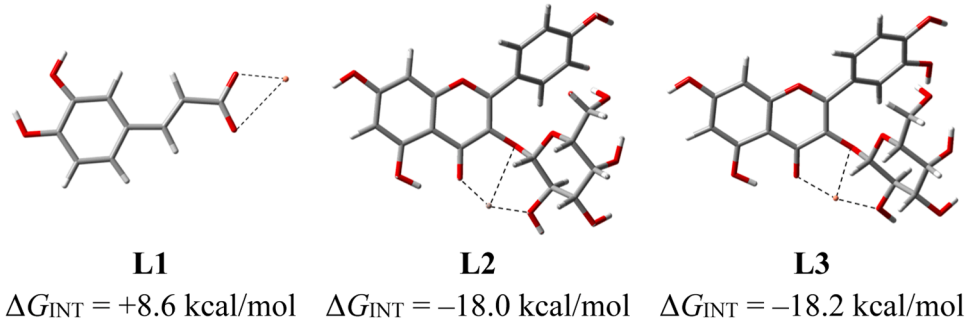

Fig. 16. Structures and interaction energies between investigated ligands and Cu(II) ions in their 1:1 complexes as obtained wth the (SMD)/M06–2X/def2-TZVP model in water.

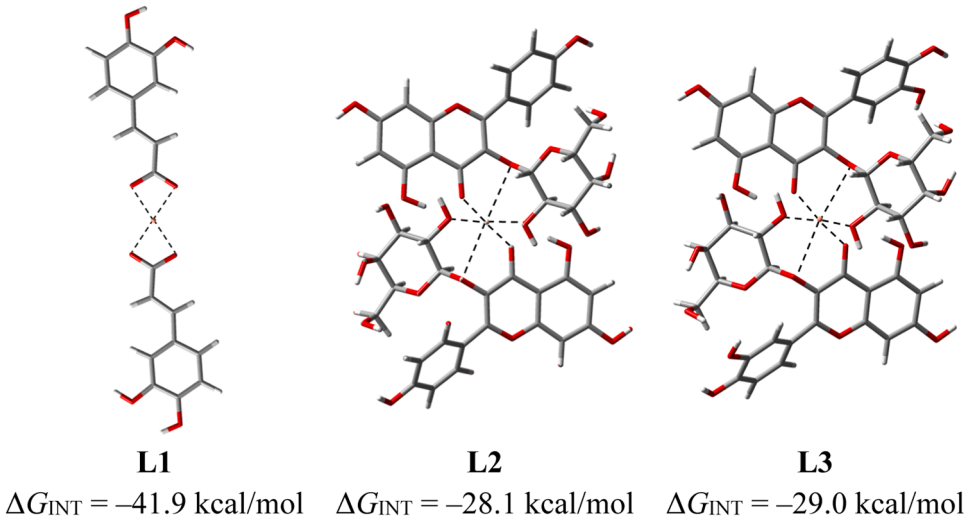

Fig. 17. Structures and interaction energies between investigated ligands and Cu(II) ions in their 2:1 complexes as obtained wth the (SMD)/M06–2X/def2-TZVP model in water.

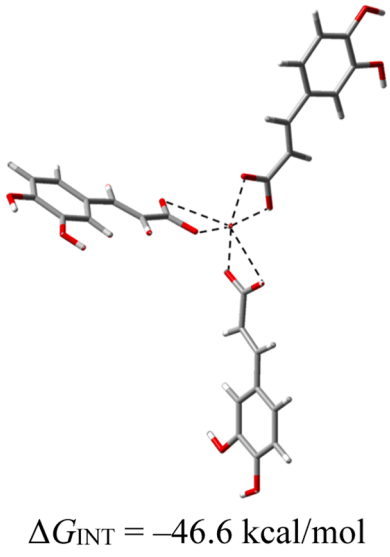

Fig. 18. Structures and interaction energy in a 3:1 complex involving caffeic acid (L1) and a Cu(II) ion as obtained wth the (SMD)/M06–2X/def2-TZVP model in water.

–OH groups and a *trans* conformation at its exocyclic double bond. **L2** and **L3**, feature intramolecular O–H···O=C hydrogen bonding within their bicyclic skeleton. Their glucoside units are oriented to form additional O–H···O=C bonds with the central carbonyl, while the three glucoside –OH groups maximize hydrogen bonding among themselves. The –CH_2–OH moiety stabilizes the phenyl ring via O–H···π interactions. The structural similarity of **L2** and **L3** supports their expected similar behavior toward Cu(II).

Feasibility assessment of Cu(II) complexation was performed by calculating interaction Gibbs free energies among components (ΔG_{INT}) for 1:1 complexes (Fig. 16). Caffeic acid (**L1**) forms an unfavorable 1:1 complex with Cu(II), seen in a positive and endergonic ΔG_{INT} = +8.6 kcal/mol, likely due to the charged nature of both components, stabilizing them in aqueous solution and hindering complexation. The most stable **L1**:Cu(II) structure shows asymmetrical binding, with Cu···O distances of 2.01 Å and 2.91 Å. A symmetrical binding mode (both Cu···O at 2.24 Å) is 1.8 kcal/mol less stable, contributing less than 5% to the solution population. In contrast, **L2** and **L3** form highly stable 1:1 complexes with Cu(II), with exergonic ΔG_{INT} values of –18.0 kcal/mol (**L2**) and –18.2 kcal/mol (**L3**). The minor difference (–0.2 kcal/mol) confirms their similar performance. Both ligands coordinate Cu(II) tridentately via (i) the bicyclic carbonyl C=O, (ii) the oxygen linking the glucoside unit, and (iii) a reoriented glucoside –OH group. Computed Cu···O distances are 1.96 Å, 2.80 Å, and 2.05 Å for **L2**, and 1.94 Å, 2.37 Å, and 2.02 Å for **L3**, with **L3** slightly shorter distances aligning with its somewhat higher interaction energy. A less stable **L3** structure, where Cu(II) binds between vicinal aromatic –OH groups, is 33.1 kcal/mol higher in energy and negligible.

Table 13
Computed energies of the frontier orbitals for identified complexes, together with their HOMO–LUMO gap as obtained with the (SMD)/M06–2X/def2-TZVP model in water.

System	*E*(HOMO) / eV	*E*(LUMO) / eV	Δ*E*(HOMO–LUMO) / eV
L1	–7.1	–0.4	6.7
1:1 complex with Cu (II)	–8.0	–1.5	6.5
2:1 complex with Cu (II)	–7.3	–1.0	6.3
3:1 complex with Cu (II)	–6.0	–1.4	4.6
L2	–7.5	–1.2	6.3
1:1 complex with Cu (II)	–7.6	–1.7	5.9
2:1 complex with Cu (II)	–7.6	–1.6	6.0
L3	–7.4	–1.2	6.2
1:1 complex with Cu (II)	–8.0	–2.0	6.0
2:1 complex with Cu (II)	–7.5	–1.6	5.9

The 2:1 ligand:Cu(II) complexes were further explored (Fig. 17). For **L2** and **L3**, hexacoordinated Cu(II) complexes are highly stable, with ΔG_{INT} values of –28.1 kcal/mol (**L2**) and –29.0 kcal/mol (**L3**), an around 60% increase from their 1:1 complexes. **L3** is slightly favored (–0.9 kcal mol^{-1}), and both ligands maintain tridentate coordination similar to their 1:1 complexes, enhancing stability. For caffeic acid (**L1**), the 2:1 complex is remarkably stable (ΔG_{INT} = –41.9 kcal/mol), surpassing **L2** and **L3** complexes. It adopts a planar geometry with four identical Cu···O distances (2.05 Å), a significant shift from the unfavorable 1:1 complex.

The bidentate carboxylate coordination of caffeic acid enables 3:1 complexes, achieving full Cu(II) hexacoordination (Fig. 18). This

complex is the most stable (ΔG_{INT} = –46.6 kcal/mol). These results suggest that at low ligand concentrations, **L2** and **L3** dominate Cu(II) complexation due to their favorable 1:1 complexes, while at higher concentrations, **L1** becomes predominant by forming highly stable 2:1 and 3:1 complexes. This concentration-dependent behavior helps explaining varying UV–Vis responses and corrosion inhibition mechanisms [11,13]. Comparison with the parent hexaaquacopper(II) complex, $[Cu(H_2O)_6]^{2+}$, which exhibits only moderate stability (ΔG_{INT} = –8.7 kcal/mol), indicates that once formed, the Cu–BLE complexes are not destabilized by surrounding water molecules and therefore remain persistent in the aqueous environment. Their stability allows them to coexist with free BLE molecules in solution and act as additional inhibiting species during adsorption onto the copper surface. Such combined action provides a rational explanation for the observed inhibition effect, particularly at higher BLE concentrations where the population of Cu–BLE complexes becomes significant.

The effect of the attached glucoside unit in **L2** and **L3** for the Cu(II) binding was investigated. For that, we repeated the analysis with model ligands **L2'** and **L3'** where the glucoside unit is replaced by the –OH group, as in original kaempferol and quercetine (Fig. S1). These ligands retain Cu(II) coordination via C=O and –OH groups but show reduced interaction energies (5–6 kcal/mol for 1:1, ~10 kcal/mol for 2:1 complexes), confirming the glucoside unit's importance for Cu(II) binding and corrosion suppression.

To validate this findings, the frontier orbital energies (HOMO and LUMO) and their differences in the complexes, correlating these with corrosion inhibition (Table 13) were examined. While HOMO and LUMO energies showed no clear trends, their difference (HOMO–LUMO gap) decreased with increasing complexation. A smaller gap indicates higher chemical reactivity, as the molecule can more readily donate electrons from its HOMO to the metal's vacant orbitals or accept electrons into its LUMO. This typically enhances the inhibitor adsorption onto the metal surface, promoting the formation of a stable protective film that shields the metal from corrosive agents like water, oxygen, or ions. Inhibitors with smaller HOMO–LUMO gaps are generally more effective, as they form stronger interactions with the metal. For instance, Obot et al. demonstrated a strong negative correlation (R^2 = 0.933) between the HOMO–LUMO gap and inhibition efficiency for benzimidazole derivatives on iron in HCl [116]. Similar findings were reported for triazole [117], furan [118] and thiadiazole [119] derivatives, where molecules with the smallest HOMO–LUMO gaps exhibited the highest corrosion inhibition efficiency. Additionally, a smaller HOMO–LUMO gap is associated with greater molecular polarizability and chemical softness, enabling better adaptation to the metal surface electronic environment. Softer, more polarizable molecules form stronger coordinate bonds with the metal, enhancing inhibition performance. While factors such as molecular size, functional groups, solubility, and the metal properties also play a role, the literature consistently highlights the HOMO–LUMO gap as a key indicator of a molecule reactivity and adsorption strength, crucial for effective corrosion inhibition. According to these insights, it can be proposed that 3:1 caffeic acid complex with Cu(II) ions likely dominates the anticorrosive features of our BLE extract, as this particular complex most easily forms in the solution and is associated with the lowest HOMO–LUMO gap (4.6 eV).

Based on previous studies on the application of BLE as a copper corrosion inhibitor in 0.5 M NaCl solution [11–13] and the results presented in this work, a schematic representation of the corrosion inhibition mechanism is shown in Fig. 19. All obtained results consistently indicate that BLE molecules and organometallic complexes adsorb on the copper surface predominantly via physical adsorption. Chemical complexation occurs between copper ions and BLE ligands in the solution phase, leading to the formation of organometallic complexes. The absence of complexes at lower BLE concentrations can be attributed to the insufficient availability of one of the reactants, as a relatively high concentration of BLE molecules is required for the spontaneous development of this type of protective system.

4. Conclusion

Blackberry leaf extract (BLE) was demonstrated to be an effective and environmentally friendly corrosion inhibitor for Cu-DHP in 0.5 M NaCl solution, achieving inhibition efficiencies up to 99.1% under

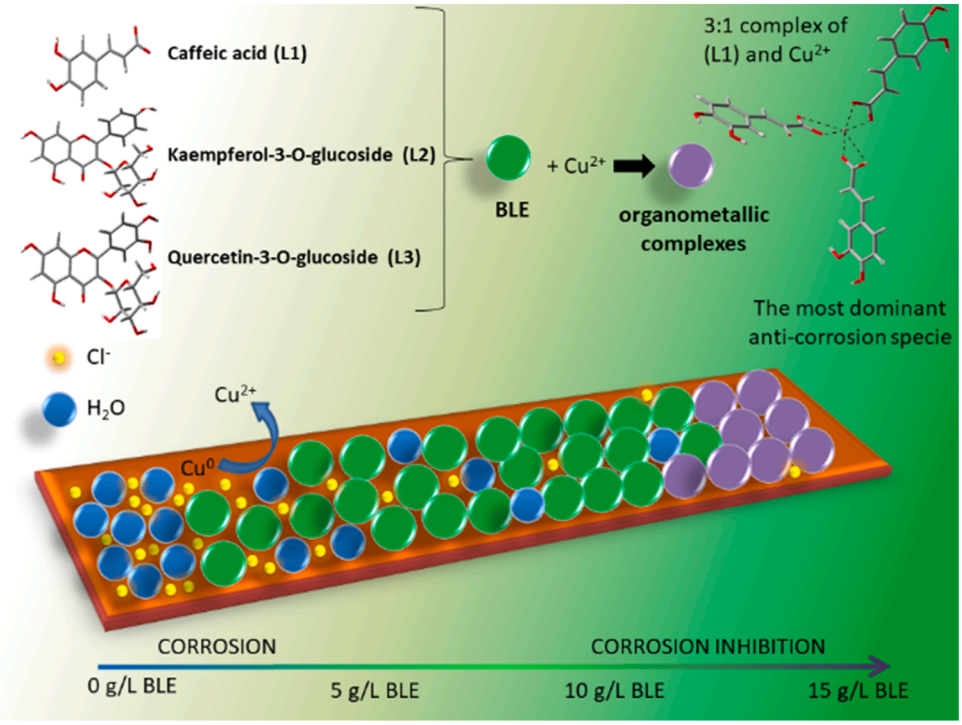

Fig. 19. Mechanism of corrosion inhibition by organic bioactive compounds of BLE and organometallic complexes involving BLE compounds and Cu(II) ion in 0.5 M NaCl solution.

optimal conditions. Electrochemical studies confirmed that BLE acts as a mixed-type inhibitor, predominantly through physical adsorption following the Langmuir isotherm. Thermodynamic parameters indicated a spontaneous and endothermic inhibition process driven by entropy increase associated with water molecule displacement from the metal surface. Optimization using response surface methodology revealed that higher BLE concentrations (15 g/L), lower temperatures (294.48 K), and longer immersion times (213.47 h) maximize inhibition performance. In addition to mechanisms commonly proposed in the literature, changes in pH and conductivity of the NaCl solution upon BLE addition, together with DFT analysis, indicated the formation of organometallic species. Stable Cu(II) complexes with caffeic acid, quercetin-3-O-glucoside, and kaempferol-3-O-glucoside were identified, with the 3:1 caffeic acid complex being dominant due to its high stability ($\Delta G_{INT} = -46.6$ kcal/mol) and low HOMO-LUMO gap, which enhance adsorption and protective film formation. The combined action of BLE components and chloride ions further strengthens inhibition, with a transition from diffusion-controlled to charge-transfer-controlled mechanisms at higher inhibitor concentrations.

This study highlights the practical and scientific value of BLE as a sustainable corrosion inhibitor and provides comprehensive insight into its electrochemical, thermodynamic, and molecular inhibition mechanisms in chloride media. The limitation of this research is based on the possibility of the existence of other compounds in BLE, considering that earlier studies showed the presence of only the three already mentioned compounds. This limits the identification of more potential organometallic complexes, as well as the potential synergistic interaction with other organic compounds in BLE. Another limitation is the range of the RSM method, where the BLE concentration range was chosen so as not to obtain negative values that need to be applied experimentally, so a more detailed explanation of the effect of BLE at concentrations below 2 g/L is currently not considered in detail.

The complexity of plant-based inhibitors lies in the fact that, unlike single-component inhibitors, their molecules interact not only with the metal surface but also with corrosive ions and metal ions generated during corrosion. The resulting organometallic complexes exhibit superior inhibitory properties compared with individual BLE molecules, which represents a novel mechanistic contribution relative to most studies on plant-based inhibitors that consider only direct molecular adsorption. Future work should therefore focus on the individual and combined effects of pure BLE constituents to identify their specific roles and possible synergistic interactions in copper corrosion protection.

CRediT authorship contribution statement

Milica Zdravković: Writing – original draft, Methodology, Investigation, Conceptualization. **Robert Vianello:** Writing – original draft, Supervision, Methodology, Investigation, Conceptualization. **Vesna Grekulović:** Writing – review & editing, Supervision, Project administration, Methodology. **Nada Štrbac:** Resources, Funding acquisition. **Bojan Zdravković:** Resources, Investigation. **Milan Gorgievski:** Validation, Data curation. **Miljan Marković:** Visualization, Software.

Declaration of competing interest

The authors declare that they have no known competing financial interests or personal relationships that could have appeared to influence the work reported in this paper.

Acknowledgment

The research presented in this paper was done with the financial support of the Ministry of Science, Technological Development and Innovation of the Republic of Serbia, within the funding of the scientific research work at the University of Belgrade - Technical Faculty in Bor, according to the contract with registration number 451-03-137/2025-03/200131. R.V. wishes to thank the Zagreb University Computing Centre (SRCE) for granting computational resources on the SUPEK supercomputer.

Supplementary materials

Supplementary material associated with this article can be found, in the online version, at doi:10.1016/j.rineng.2026.109812.

Data availability

Data will be made available on request.

References

[1] B. Tan, H. Ren, R. Zhang, R. Wang, L. Ma, X. Li, W. Li, L. Guo, M.K. Al-Sadoon, A novel corrosion inhibitor for copper in sulfuric acid media: complexation of iodide ions with Benincasa Hispida leaf extract, Colloids Surf. A Physicochem. Eng. Asp. 705 (Part 2) (2025) 135710, https://doi.org/10.1016/j.colsurfa.2024.135710.

[2] O.O. Ekerenam, A.I. Ikeuba, C.N. Njoku, D.I. Njoku, W. Emori, I.K. Nwokolo, I.I. N. Etim, B.O. Okonkwo, I.I. Udoh, E.F. Daniel, P.C. Uzoma, B.O. Awonusi, S. K. Kolawole, I.P. Etim, O.S. Olanrele, Advancements in corrosion studies and protective measures for copper and copper-based alloys in varied environmental conditions, Results Eng. 26 (2025) 105257, https://doi.org/10.1016/j.rineng.2025.105257.

[3] H. Kwiatkowski, S. Krakowiak, Ł. Gaweł, Vitamin B9 as a new eco-friendly corrosion inhibitor for copper in 3.5% NaCl solution, J. Ind. Eng. Chem. 142 (2025) 282–292, https://doi.org/10.1016/j.jiec.2024.07.035.

[4] X. Li, D. Zhang, Z. Liu, Z. Li, C. Du, C. Dong, Materials science: share corrosion data, Nature 527 (7579) (2015) 441–442.

[5] X. Sun, H. Tian, X. Ma, W. Li, A. Zhang, L. Guo, H. Zhu, B. Hou, Insight into the inhibition ability of *Eupatorium adenoprum* leaves extract as an efficiency corrosion inhibitor for copper in acid solution, Green Chem. Lett. Rev. 18 (1) (2024) 2441217, https://doi.org/10.1080/17518253.2024.2441217.

[6] R.K. Ahmed, S. Zhang, *Alchemilla Vulgaris* extract as green inhibitor of copper corrosion in hydrochloric acid, Int. J. Electrochem. Sci. 14 (2019) 10657–10669, https://doi.org/10.20964/2019.11.43.

[7] N. Kavitha, J. Ravichandran, A. Murugesh, An eco-friendly *Leucas aspera* leaves extract inhibitor for copper corrosion in hydrochloric acid medium, J. Bio Tribo Corros. 6 (4) (2020) 103, https://doi.org/10.1007/s40735-020-00400-8.

[8] A. Jmiai, A. Tara, S. El Issami, M. Hilali, O. Jbara, L. Bazzi, A new trend in corrosion protection of copper in acidic medium by using Jujube shell extract as an effective green and environmentally safe corrosion inhibitor: experimental, quantum chemistry approach and Monte Carlo simulation study, J. Mol. Liq. 322 (08) (2020) 114509, https://doi.org/10.1016/j.molliq.2020.114509.

[9] M.A. Deyab, Egyptian licorice extract as a green corrosion inhibitor for copper in hydrochloric acid solution, J. Ind. Eng. Chem. 22 (2015) 384, https://doi.org/10.1016/j.jiec.2014.07.036.

[10] M. Keramatinia, M. Ramezanzadeh, G. Bahlakeh, B. Ramezanzadeh, Synthesis of a multi-functional zinc-centered nitrogen-rich graphene-like thin film from natural sources on the steel surface for achieving superior anti-corrosion properties, Corros. Sci. 178 (2021) 109077, https://doi.org/10.1016/j.corsci.2020.109077.

[11] M. Zdravković, V. Grekulović, J. Suljagić, N. Štrbac, I. Marković, M. Gorgievski, M. Marković, The Rubus fruticosus leaf extract as an eco-friendly copper corrosion inhibitor, Prot. Met. Phys. Chem. Surf. (2024), https://doi.org/10.1134/S2070205124701843, pp. 544-453.

[12] M. Zdravković, V. Grekulović, J. Suljagić, D. Stanković, S. Savić, M. Radovanović, U. Stamenković, Influence of blackberry leaf extract on the copper corrosion behaviour in 0.5 M NaCl, Bioelectrochemistry 151 (2023), https://doi.org/10.1016/j.bioelechem.2023.108401.

[13] M. Zdravković, V. Grekulović, E. Huseinović, R. Vianello, N. Štrbac, M. Huremović, M. Gorgievski, Uv-vis identification of copper complexes with inhibitor organic components in the electrolyte, in: Proceedings of the XVI IMPRC, Belgrade, 2025, https://doi.org/10.5937/IMPRC25226Z.

[14] S. Sheetal Kundu, S. Thakur, A.K. Singh, M. Singh, B. Pani, V.S. Saji, A review of electrochemical techniques for corrosion monitoring–Fundamentals and research updates, Crit. Rev. Anal. Chem. 55 (1) (2023) 161–186, https://doi.org/10.1080/10408347.2023.2267671.

[15] M.E. Mert, C. Güngör, B.D. Mert, Analytical study on mild steel corrosion inhibition in acidic environment: DFT modeling and RSM optimization, Fuel 381 (Part D) (2025) 133729, https://doi.org/10.1016/j.fuel.2024.133729.

[16] Y. Tan, J. Qin, S. Chang, S. Ma, L. Su, N. Liu, Q. Zhao, X. Wang, C. Li, J. Ma, K. Wu, Z. Ye, Integrated response surface and machine learning approach: experimental optimization and DFT analysis for NaN3 removal via NaClO oxidation, J. Water Process Eng. 70 (2025) 107067, https://doi.org/10.1016/j.jwpe.2025.107067.

[17] C. Wang, E. Yang, Experimental and computational studies of cationic Gemini surfactants as corrosion inhibitors for carbon steel in 15% HCl, Phys. Chem. Chem. Phys. 27 (3) (2025) 1378–1393.

[18] O.D. Onukwuli, I.A. Nnanwube, F.O. Ochili, M. Omotioma, DFT, experimental and optimization studies on the corrosion inhibition of aluminium in H2SO4 with danacid as inhibitor, Results Eng. 24 (2024) 103113, https://doi.org/10.1016/j.rineng.2024.103113.

[19] I. Veza, M. Spraggon, I.M.R. Fattah, M. Idris, Response surface methodology (RSM) for optimizing engine performance and emissions fueled with biofuel: review of RSM for sustainability energy transition, Results Eng. 18 (2023) 101213, https://doi.org/10.1016/j.rineng.2023.101213.

[20] S. Ahmadi, A. Khormali, Optimization of the corrosion inhibition performance of 2-mercaptobenzothiazole for carbon steel in HCl media using response surface methodology, Fuel 357 (Part A) (2024) 129783, https://doi.org/10.1016/j.fuel.2023.129783.

[21] F.O. Edoziuno, A.A. Adediran, B.U. Odoni, A.D. Akinwekomi, O.S. Adesina, M. Oki, G. Brando, Optimization and development of predictive models for the corrosion inhibition of mild steel in sulphuric acid by methyl-5-benzoyl-2-benzimidazole carbamate (mebendazole), Cogent Eng. 7 (1) (2020), https://doi.org/10.1080/23311916.2020.1714100.

[22] D.I. Udunwa, O.D. Onukwuli, V.C. Anadebe, Synthesis and evaluation of 1-butyl-3-methylimidazolium chloride based ionic liquid for acid corrosion inhibition of aluminum alloy: empirical, DFT/MD-simulation and RSM modeling, J. Mol. Liq. 364 (2022) 120019, https://doi.org/10.1016/j.molliq.2022.120019.

[23] T. Gu, Z. Chen, X. Jiang, L. Zhou, Y. Liao, M. Duan, H. Wang, Q. Pu, Synthesis and inhibition of N-alkyl-2-(4-hydroxybut-2-ynyl) pyridinium bromide for mild steel in acid solution: box–Behnken design optimization and mechanism probe, Corros. Sci. 90 (2015) 118–132, https://doi.org/10.1016/j.corsci.2014.10.004.

[24] L.N. Emembolu, P.E. Ohale, C.E. Onu, N.J. Ohale, Comparison of RSM and ANFIS modeling techniques in corrosion inhibition studies of Aspilia Africana leaf extract on mild steel and aluminium metal in acidic medium, Appl. Surf. Sci. Adv. 11 (2022) 100316, https://doi.org/10.1016/j.apsadv.2022.100316.

[25] K.H. Goh, T.T. Lim, P.C. Chui, Evaluation of the effect of dosage, pH and contact time on high-dose phosphate inhibition for copper corrosion control using response surface methodology (RSM), Corros. Sci. 50 (4) (2008) 918–927, https://doi.org/10.1016/j.corsci.2007.12.008.

[26] F.S. de Souza, A. Spinelli, Caffeic acid as a green corrosion inhibitor for mild steel, Corros. Sci. 51 (3) (2009) 642–649, https://doi.org/10.1016/j.corsci.2008.12.013.

[27] A.M. Fekry, R.R. Mohamed, Acetyl thiourea chitosan as an eco-friendly inhibitor for mild steel in sulphuric acid medium, Electrochim. Acta 55 (2010) 1933–1939, https://doi.org/10.1016/j.electacta.2009.11.011.

[28] Y. Qiang, S. Zhang, B. Tan, S. Chen, Evaluation of ginkgo leaf extract as an eco-friendly corrosion inhibitor of X70 steel in HCl solution, Corros. Sci. 133 (2018) 6–16, https://doi.org/10.1016/j.corsci.2018.01.008.

[29] Z.A. Mas'ud, N. Darmawan, J. Dawolo, Y.B. Apriliyanto, Fatty amidine as copper corrosion inhibitor, J. Chem. 2020 (2020) 1092643, https://doi.org/10.1155/2020/1092643.

[30] I.B. Obot, N.O. Obi-Egbedi, Adsorption properties and inhibition of mild steel corrosion in sulphuric acid solution by ketoconazole: experimental and theoretical investigation, Corros. Sci. 52 (2010) 198–204, https://doi.org/10.1016/j.corsci.2009.09.002.

[31] I. Dhouibi, F. Masmoudi, M. Bouaziz, M. Masmoudi, A study of the anti-corrosive effects of essential oils of rosemary and myrtle for copper corrosion in chloride media, Arab. J. Chem. 14 (2021) 102961, https://doi.org/10.1016/j.arabjc.2020.102961.

[32] G. Mu, X. Li, G. Liu, Synergistic inhibition between tween 60 and NaCl on the corrosion of cold rolled steel in 0.5 M sulfuric acid, Corros. Sci. 47 (2005) 1932–1952, https://doi.org/10.1016/j.corsci.2004.09.020.

[33] H.S. Gadow, M.M. Motaweab, H.M. Elabbasyc, Investigation of myrrh extract as a new corrosion inhibitor for α-brass in 3.5% NaCl solution polluted by 16 ppm sulfide, RSC Adv. 7 (2017) 29883–29898, https://doi.org/10.1039/C7RA04271J.

[34] H.S. Gadow, T.A. Farghaly, A.M. Eldesoky, Experimental and theoretical investigations for some spiropyrazoles derivatives as corrosion inhibitors for copper in 2 M HNO_3 solutions, J. Mol. Liq. 294 (2019) 111614, https://doi.org/10.1016/j.molliq.2019.111614.

[35] K.S. Sudhish, E.E. Eno, Corrosion inhibition, adsorption behavior and thermodynamic properties of streptomycin on mild steel in hydrochloric acid medium, Int. J. Electrochem. Sci. 6 (8) (2011) 3277–3291, https://doi.org/10.1016/S1452-3981(23)18251-4.

[36] S. Manimegalai, P. Manjula, Thermodynamic and adsorption studies for corrosion inhibition of mild steel in aqueous media by *Sargasam swartzii* (Brown algae), J. Mater. Environ. Sci. 6 (6) (2015) 1629–1637.

[37] J.M. Thomas, W.J. Thomas, Introduction to the Principles of Heterogeneous Catalysis, 5th edn, Academic Press, London, 1981.

[38] N.M. Amadi, J.O. Ezeugo, C.C. Okoye, J.I. Obibuenyi, M.A. Chidiebere, D. O. Onukwuli, V.C. Anadebe, 1-Hexadecyl-3-methylimidazolium tetrachloroindate ionic liquid as corrosion inhibitor for mild steel: insight from experimental, computational, multivariate statistics and multi-quadratic regression based machine learning model, Results Eng. 24 (2024) 103115, https://doi.org/10.1016/j.rineng.2024.103115.

[39] H. Ashassi-Sorkhabi, Z. Ghasemi, D. Seifzadeh, The inhibition effect of some amino acids towards the corrosion of aluminum in 1 M HCl + 1 M H_2SO_4 solution, Appl. Surf. Sci. 249 (1–4) (2005) 408–418, https://doi.org/10.1016/j.apsusc.2004.12.016.

[40] N.O. Eddy, S.A. Odoemelam, A.O. Odiongenyi, Inhibitive, adsorption and synergistic studies on ethanol extract of *Gnetum africana* as green corrosion inhibitor for mild steel in H_2SO_4, Green Chem. Lett. Rev. (2) (2009) 111–119, https://doi.org/10.1080/17518250903170868.

[41] D. Daoud, T. Douadi, H. Hamani, S. Chafaa, M. Al-Noaimi, Corrosion inhibition of mild steel by two new S-heterocyclic compounds in 1 M HCl: experimental and computational study, Corros. Sci. 94 (2015) 21–37, https://doi.org/10.1016/j.corsci.2015.01.025.

[42] R.K. Ahmeda, S. Zhang, *Atriplex leucoclada* extract: a promising eco-friendly anticorrosive agent for copper in aqueous media, J. Ind. Eng. Chem. 99 (2021) 334–343, https://doi.org/10.1016/j.jiec.2021.04.042.

[43] Z.M. Hadi, J. Al-Sawaad, Thermodynamic and quantum chemistry study for dimethylol-5-methyl hydantoin and its derivatives as corrosion inhibitors for carbon steel N-80 in raw water (cooling water system), J. Mater. Environ. Sci. 2 (2) (2011) 128–147.

[44] A. Amin, K.F. Khaled, Q. Mohsen, A. Arida, A study of the inhibition of iron corrosion in HCl solutions by some amino acids, Corros. Sci. 52 (5) (2010) 1684–1695, https://doi.org/10.1016/j.corsci.2010.01.019.

[45] S.A. Umoren, O. Ogbobe, I.O. Igwe, E.E. Ebenso, Inhibition of mild steel corrosion in acidic medium using synthetic and naturally occurring polymers and synergistic halide additives, Corros. Sci. 50 (2008) 1998–2006, https://doi.org/10.1016/j.corsci.2008.04.015.

[46] M. Darvishmotevalli, A. Zarei, M. Moradnia, M. Noorisepehr, H. Mohammadi, Optimization of saline wastewater treatment using electrochemical oxidation process: prediction by RSM method, MethodsX 6 (2019) 1101–1113, https://doi.org/10.1016/j.mex.2019.03.015.

[47] A.A. Mohammadi, A. Zarei, H. Alidadi, M. Afsharnia, M. Shams, Two-dimensional zeolitic imidazolate framework-8 for efficient removal of phosphate from water, process modeling, optimization, kinetic, and isotherm studies, Desalin. Water Treat. 129 (2018) 244–254.

[48] P. Pracht, F. Bohle, S. Grimme, Automated exploration of the low-energy chemical space with fast quantum chemical methods, Phys. Chem. Chem. Phys. 22 (2020) 7169–7192, https://doi.org/10.1039/C9CP06869D.

[49] C. Bannwarth, S. Ehlert, S. Grimme, GFN2-xTB - an accurate and broadly parametrized self-consistent tight-binding quantum chemical method with multipole electrostatics and density-dependent dispersion contributions, J. Chem. Theory Comput. 15 (3) (2019) 1652–1671, https://doi.org/10.1021/acs.jctc.8b01176.

[50] A.V. Onufriev, D.A. Case, Generalized born implicit solvent models for biomolecules, Annu. Rev. Biophys. 48 (2019) 275–296, https://doi.org/10.1146/annurev-biophys-052118-115325.

[51] S. Grimme, Exploration of chemical compound, conformer, and reaction space with meta-dynamics simulations based on tight-binding quantum chemical calculations, J. Chem. Theory Comput. 15 (5) (2019) 2847–2862, https://doi.org/10.1021/acs.jctc.9b00143.

[52] M. Bursch, J.M. Mewes, A. Hansen, S. Grimme, Best-practice DFT protocols for basic molecular computational chemistry, Angew. Chem. Int. Ed. 134 (42) (2022) e202205735, https://doi.org/10.1002/anie.202205735.

[53] N.P. Juraj, T. Tandarić, V. Tadić, B. Perić, D. Moreth, U. Schatzschneider, A. Brozović, R. Vianello, S.I. Kirin, Tuning the coordination properties of chiral pseudopeptide bis(2-picolyl)amine and iminodiacetamide ligands in Zn(II) and Cu(II) complexes, Dalton Trans. 51 (2022) 17008–17021, https://doi.org/10.1039/D2DT02895F.

[54] N. Pantalon Juraj, G.I. Miletić, B. Perić, Z. Popović, N. Smrečki, R. Vianello, S. I. Kirin, Stereochemistry of hexacoordinated Zn(II), Cu(II), Ni(II), and Co(II) complexes with iminodiacetamide ligands, Inorg. Chem. 58 (2019) 16445–16457, https://doi.org/10.1021/acs.inorgchem.9b02200.

[55] N. Pantalon Juraj, M. Krklec, T. Novosel, B. Perić, R. Vianello, S. Raić-Malić, S. I. Kirin, Copper(II) and zinc(II) complexes of mono- and bis-1,2,3-triazole-substituted heterocyclic ligands, Dalton Trans. 49 (2020) 9002–9015, https://doi.org/10.1039/D0DT01244K.

[56] M.J. Frisch, G.W. Trucks, H.B. Schlegel, G.E. Scuseria, M.A. Robb, J. R. Cheeseman, G. Scalmani, V. Barone, G.A. Petersson, H. Nakatsuji, X. Li, M. Caricato, A.V. Marenich, J. Bloino, B.G. Janesko, R. Gomperts, B. Mennucci, H. P. Hratchian, J.V. Ortiz, A.F. Izmaylov, J.L. Sonnenberg, D. Williams-Young, F. Ding, F. Lipparini, F. Egidi, J. Goings, B. Peng, A. Petrone, T. Henderson, D. Ranasinghe, V.G. Zakrzewski, J. Gao, N. Rega, G. Zheng, W. Liang, M. Hada, M. Ehara, K. Toyota, R. Fukuda, J. Hasegawa, M. Ishida, T. Nakajima, Y. Honda, O. Kitao, H. Nakai, T. Vreven, K. Throssell, J.A. Montgomery Jr., J.E. Peralta, F. Ogliaro, M.J. Bearpark, J.J. Heyd, E.N. Brothers, K.N. Kudin, V.N. Staroverov, T.A. Keith, R. Kobayashi, J. Normand, K. Raghavachari, A.P. Rendell, J.C. Burant, S.S. Iyengar, J. Tomasi, M. Cossi, J.M. Millam, M. Klene, C. Adamo, R. Cammi, J. W. Ochterski, R.L. Martin, K. Morokuma, O. Farkas, J.B. Foresman, D.J. Fox, Gaussian 16, Revision C.01, Gaussian, Inc., Wallingford, 2016.

[57] F. Arjmand, A. Adriaens, Influence of pH and chloride concentration on the corrosion behavior of unalloyed copper in NaCl solution: a comparative study between the micro and macro scales, Materials 5 (2012) 2439–2464, https://doi.org/10.3390/ma5122439.

[58] G.K. Glass, C.L. Page, N.R. Short, Factors affecting the corrosion rate of steel in carbonated mortars, Corros. Sci. 32 (12) (1991) 1283–1294, https://doi.org/10.1016/0010-938X(91)90048-T.

[59] M.R. Olthof, P.C.H. Hollman, T.B. Vree, M.B. Katan, Bioavailabilities of quercetin-3-glucoside and quercetin-4′-glucoside do not differ in humans, J. Nutr. 130 (5) (2000) 1200–1203, https://doi.org/10.1093/jn/130.5.1200.

[60] A.G. Junior, F.M. Gasparotto, M.A. Boffo, E.L.B. Lourenço, M.É.A. Stefanello, M. J. Salvador, J.E. da Silva-Santos, M.C.A. Marques, C.A.L. Kassuya, Diuretic and potassium-sparing effect of isoquercitrin–An active flavonoid of *Tropaeolum majus L*, J. Ethnopharmacol. 134 (2) (2011) 210–215, https://doi.org/10.1016/j.jep.2010.12.009.

[61] S.A. Umoren, M.M. Solomon, Effect of halide ions on the corrosion inhibition efficiency of different organic species–A review, J. Ind. Eng. Chem. 21 (2015) 81–100, https://doi.org/10.1016/j.jiec.2014.09.033.
[62] E.E. Oguzie, A.I. Onuchukwu, P.C. Okafor, E.E. Ebenso, Corrosion inhibition and adsorption behaviour of *Ocimum basilicum* extract on aluminium, Pigment Resin Technol. 35 (2) (2006) 63–70, https://doi.org/10.1108/03699420610652340.
[63] E.E. Oguzie, Influence of halide ions on the inhibitive effect of congo red dye on the corrosion of mild steel in sulphuric acid solution, Mater. Chem. Phys. 87 (1) (2004) 212–217, https://doi.org/10.1016/j.matchemphys.2004.06.006.
[64] M. Hidalgo, C. Sánchez-Moreno, S. de Pascual-Teresa, Flavonoid–flavonoid interaction and its effect on their antioxidant activity, Food Chem. 121 (3) (2010) 691–696, https://doi.org/10.1016/j.foodchem.2009.12.097.
[65] M.L. Guo, C. Perez, Y.B. Wei, E. Rapoza, G. Su, F. Bou-Abdallah, N.D. Chasteen, Iron-binding properties of plant phenolics and cranberry's bio-effects, Dalton Trans. 10 (2007) 4951–4961, https://doi.org/10.1039/B705136K.
[66] R.D. Horniblow, D. Henesy, T.H. Iqbal, C. Tselepis, Modulation of iron transport, metabolism and reactive oxygen status by quercetin-iron complexes *in vitro*, Mol. Nutr. Food Res. 61 (3) (2016), https://doi.org/10.1002/mnfr.201600692.
[67] A. Miličević, N. Raos, Modelling of protective mechanism of iron(II)-polyphenol binding with OH-related molecular descriptors, Croat. Chem. Acta 89 (4) (2016), https://doi.org/10.5562/cca2996.
[68] C.A. Perez, Y. Wei, M. Guo, Iron-binding and anti-fenton properties of baicalein and baicalin, J. Inorg. Biochem. 103 (2009) 326–332, https://doi.org/10.1016/j.jinorgbio.2008.11.003.
[69] Z. Kejik, R. Kaplanek, M. Masarik, P. Babula, A. Matkowski, P. Filipensky, K. Vesela, J. Gburek, D. Sykora, P. Martasek, M. Jakubek, Iron complexes of flavonoids-antioxidant capacity and beyond, Int. J. Mol. Sci. 22 (2) (2021) 646, https://doi.org/10.3390/ijms22020646.
[70] L. Mira, M. Tereza Fernandez, M. Santos, R. Roch, M. Helena Florêncı, K. R. Jennings, Interactions of flavonoids with iron and copper ions: a mechanism for their antioxidant activity, Free Radic. Res. 36 (11) (2002) 1199–1208, https://doi.org/10.1080/1071576021000016463.
[71] A.M. Alfantazi, T.M. Ahmed, D. Tromans, Corrosion behavior of copper alloys in chloride media, Mater. Des. 30 (7) (2009) 2425–2430, https://doi.org/10.1016/j.matdes.2008.10.015.
[72] Y. Liu, M. Guo, Studies on transition metal-quercetin complexes using electrospray ionization tandem mass spectrometry, Molecules 20 (2015) 8583–8594, https://doi.org/10.3390/molecules20058583.
[73] J. Lee, O.H. Kim, B.K. Jung, I.S. Cho, Y.J. Lee, H.J. Choi, Y.C. Kim, Y.H. Oh, K. Jung, S.H. Cha, K.I. Jang, Influence of mineral supplementation on the results from analysis of flavonol glycoside content in *ginkgo biloba* dietary supplements, Prev. Nutr. Food Sci. 24 (2019), https://doi.org/10.3746/pnf.2019.24.1.75.
[74] M.C. Catapano, V. Tvrdý, J. Karlíčková, T. Migkos, K. Valentová, V. Křen, P. Mladěnka, The stoichiometry of isoquercitrin complex with iron or copper is highly dependent on experimental conditions, Nutrients 9 (11) (2017) 1193, https://doi.org/10.3390/nu9111193.
[75] A. Pekal, M. Biesaga, K. Pyrzynska, Interaction of quercetin with copper ions: complexation, oxidation and reactivity towards radicals, Biometals 24 (2011) 41–49, https://doi.org/10.1007/s10534-010-9372-7.
[76] M. Simunkova, Z. Barbierikova, K. Jomova, L. Hudecova, P. Lauro, S.H. Alwasel, I. Alhazza, C.J. Rhodes, M. Valko, Antioxidant vs. Prooxidant properties of the flavonoid, kaempferol, in the presence of Cu(II) ions: a ROS-scavenging activity, fenton reaction and DNA damage study, Int. J. Mol. Sci. 22 (4) (2021) 1619, https://doi.org/10.3390/ijms22041619.
[77] S. Lyu, W. Wang, Spectroscopic methodologies and computational simulation studies on the characterization of the interaction between human serum albumin and astragalin, J. Biomol. Struct. Dyn. 39 (8) (2020) 2959–2970, https://doi.org/10.1080/07391102.2020.1758213.
[78] C. De Stefano, C. Foti, O. Giuffrè, S. Sammartano, Acid–base and UV behavior of 3-(3,4-dihydroxyphenyl)-propenoic acid (caffeic acid) and complexing ability towards different divalent metal cations in aqueous solution, J. Mol. Liq. 195 (2014) 9–16, https://doi.org/10.1016/j.molliq.2014.01.027.
[79] H. Irving, R.J.P. Williams, The stability of transition-metal complexes, J. Chem. Soc. (1953) 3192–3210, https://doi.org/10.1039/JR9530003192.
[80] J.J.L. Cilliers, V.L. Singleton, Characterization of the products of nonenzymic autoxidative phenolic reactions in a caffeic acid model system, Agric. Food Chem. 39 (7) (1991) 1298–1303, https://doi.org/10.1021/jf00007a021.
[81] P. Mourya, P. Singh, A.K. Tewari, R.B. Rastogi, M.M. Singh, Relationship between structure and inhibition behaviour of quinolinium salts for mild steel corrosion: experimental and theoretical approach, Corros. Sci. 95 (2015) 71–87, https://doi.org/10.1016/j.corsci.2015.02.034.
[82] M. Mobin, S. Zehra, M. Parveen, L-Cysteine as corrosion inhibitor for mild steel in 1M HCl and synergistic effect of anionic, cationic and non-ionic surfactants, J. Mol. Liq. 216 (2016) 598–607, https://doi.org/10.1016/j.molliq.2016.01.087.
[83] E.I. Ating, S.A. Umoren, I.I. Udousoro, E.E. Ebenso, A.P. Udoh, Leaves extract of *Ananas sativum* as green corrosion inhibitor for aluminium in hydrochloric acid solutions, Green Chem. Lett. Rev. 3 (2) (2010) 61–68, https://doi.org/10.1080/17518250903505253.
[84] N.I. Kairi, J. Kassim, The effect of temperature on the corrosion inhibition of mild steel in 1 M HCl solution by *Curcuma Longa* extract, Int. J. Electrochem. Sci. 8 (5) (2013) 7138–7155, https://doi.org/10.1016/S1452-3981(23)14836-X.
[85] A. Miralrio, A.E. Vázquez, Plant extracts as green corrosion inhibitors for different metal surfaces and corrosive media: a review, Processes 8 (8) (2020) 942, https://doi.org/10.3390/pr8080942.
[86] G. Vastag, J. Nakomčić, A. Shaban, Thermodynamic properties of 5-(4′-isopropylbenzylidene)-2,4-dioxotetrahydro-1,3-thiazole as a corrosion inhibitor for copper in acid solution, Int. J. Electrochem. Sci. 11 (10) (2016) 8229–8244, https://doi.org/10.20964/2016.10.27.
[87] R. Solmaz, Investigation of the inhibition effect of 5-((E)-4-phenylbuta-1,3-dienylideneamino)-1,3,4-thiadiazole-2-thiol Schiff base on mild steel corrosion in hydrochloric acid, Corros. Sci. 52 (10) (2010) 3321–3330, https://doi.org/10.1016/j.corsci.2010.06.001.
[88] A. Mishra, J. Aslam, C. Verma, M.A. Quraishi, E.E. Ebenso, Imidazoles as highly effective heterocyclic corrosion inhibitors for metals and alloys in aqueous electrolytes: a review, J. Taiwan Inst. Chem. Eng. 114 (2020) 341–358, https://doi.org/10.1016/j.jtice.2020.08.034.
[89] M.I. Awad, Eco friendly corrosion inhibitors: inhibitive action of quinine for corrosion of low carbon steel in 1 m HCl, J. Appl. Electrochem. 36 (2006) 1163–1168, https://doi.org/10.1007/s10800-006-9204-1.
[90] A. Popova, E. Sokolova, S. Raicheva, M. Christov, AC and DC study of the temperature effect on mild steel corrosion in acid Media in the presence of benzimidazole derivatives, Corros. Sci. 45 (2003) 33–58, https://doi.org/10.1016/S0010-938X(02)00072-0.
[91] T. Szauer, A. Brandt, Adsorption of oleates of various amines on iron in acidic solution, Electrochim. Acta 26 (9) (1981) 1253–1256, https://doi.org/10.1016/0013-4686(81)85107-9.
[92] F. Bentiss, M. Lebrini, M. Lagrenée, Thermodynamic characterization of metal dissolution and inhibitor adsorption processes in mild steel/2,5-bis(n-thienyl)-1,3,4-thiadiazoles/hydrochloric acid system, Corros. Sci. 47 (12) (2005) 2915–2931, https://doi.org/10.1016/j.corsci.2005.05.034.
[93] P. Refait, C. Rahal, M. Masmoudi, Corrosion inhibition of copper in 0.5 M NaCl solutions by aqueous and hydrolysis acid extracts of olive leaf, J. Electroanal. Chem. 859 (2020) 113834, https://doi.org/10.1016/j.jelechem.2020.113834.
[94] A.M. Badiea, K.N. Mohana, Effect of temperature and fluid velocity on corrosion mechanism of low carbon steel in presence of 2-hydrazino-4,7-dimethylbenzo-thiazole in industrial water medium, Corros. Sci. 51 (9) (2009) 2231–2241, https://doi.org/10.1016/j.corsci.2009.06.011.
[95] S. Deng, X. Li, X. Xie, Hydroxymethyl urea and 1,3-bis(hydroxymethyl) urea as corrosion inhibitors for steel in HCl solution, Corros. Sci. 80 (2014) 276–289, https://doi.org/10.1016/j.corsci.2013.11.041.
[96] B.G. Ateya, B.E. El-Anadouli, F.M. El-Nizamy, The adsorption of thiourea on mild steel, Corros. Sci. 24 (6) (1984) 509–515, https://doi.org/10.1016/0010-938X(84)90033-7.
[97] A.M.A. Muhammad, N.A. Mohammad, I.M. Izan, P. Hariy, N. Erna, Gravimetric and electrochemical statistical optimizations for improving copper corrosion resistance in hydrochloric acid using thiosemicarbazone-linked 3-acetylpyridine, RSC Adv. 12 (2022) 27793–27808, https://doi.org/10.1039/D2RA05192C.
[98] M. Qasemi, A. Zarei, M. Afsharnia, R. Salehi, M. Allahdadi, M. Farhang, Data on cadmium removal from synthetic aqueous solution using garbage ash, Data Brief 20 (2018) 1115–1123, https://doi.org/10.1016/j.dib.2018.08.163.
[99] H. Mirhosseini, C.P. Tan, A.R. Taherian, H.C. Boo, Modeling the physicochemical properties of orange beverage emulsion as function of main emulsion components using response surface methodology, Carbohydr. Polym. 75 (2009) 512–520, https://doi.org/10.1016/j.carbpol.2008.08.022.
[100] M.J. Bashir, H.A. Aziz, M.S. Yusoff, M.N. Adlan, Application of response surface methodology (RSM) for optimization of ammoniacal nitrogen removal from semi-aerobic landfill leachate using ion exchange resin, Desalination 254 (2010) 154–161, https://doi.org/10.1016/j.desal.2009.12.002.
[101] 2024. https://support.minitab.com/.
[102] M.A. Bezerra, R.E. Santelli, E.P. Oliveira, L.S. Villar, L.A. Escaleira, Response surface methodology (RSM) as a tool for optimization in analytical chemistry, Talanta 76 (5) (2008) 965–977, https://doi.org/10.1016/j.talanta.2008.05.019.
[103] M.S.S.M. Meiabadi, A. Kazerooni, M. Moradi, M.J. Torkamany, Laser assisted joining of St12 to polycarbonate: experimental study and numerical simulation, Optik 208 (2020) 164151, https://doi.org/10.1016/j.ijleo.2019.164151.
[104] G.D. Suditu, A.C. Blaga, R.E. Tataru-Farmus, C. Zaharia, D. Suteu, Statistical analysis and optimization of the brilliant red HE-3B dye biosorption onto a biosorbent based on residual biomass, Materials 15 (20) (2022) 7180, https://doi.org/10.3390/ma15207180.
[105] A.L. Ahmad, S. Ismail, S. Bhatia, Optimization of coagulation-flocculation process for palm oil mill effluent using response surface methodology, Environ. Sci. Technol. 39 (8) (2005) 2828–2834, https://doi.org/10.1021/es0498080.
[106] A. Zarrouk, I. Warad, B. Hammouti, A. Dafali, S.S. Al-Deyab, N. Benchat, The effect of temperature on the corrosion of Cu/HNO_3 in the presence of organic inhibitor: part-2, Int. J. Electrochem. Sci. 5 (10) (2010) 1516–1526, https://doi.org/10.1016/S1452-3981(23)15378-8.
[107] M.C.S. Inacio, E.W. Paxton, S.E. Graves, R.S. Namba, S. Nemes, Projected increase in total knee arthroplasty in the United States - an alternative projection model, Osteoarthr. Cartil. 25 (11) (2017) 1797–1803, https://doi.org/10.1016/j.joca.2017.07.022.
[108] G.A. Kelley, K.S. Kelley, B.L. Stauffer, Resistance training and inter-interindividual response differences on cardiorespiratory fitness in older adults: an ancillary meta-analysis of randomized controlled trials, Sci. Prog. 107 (1) (2024), https://doi.org/10.1177/00368504241227088.
[109] M.N. Mona, A.G. Ghalia, S.I.A. Amal, S.F. Abd El Aziz, Application of lentil seed extract as an inhibitor to assess the corrosion properties of copper–nickel alloys in a NaCl environment, RSC Adv. 14 (38) (2024) 28044–28057, https://doi.org/10.1039/d4ra04758c.
[110] I.M. Ritchie, S. Bailey, R. Woods, The metal–solution interface, Adv. Colloid Interface Sci. 80 (3) (1999) 183–231, https://doi.org/10.1016/S0001-8686(98)00082-7.

[111] L. Vrsalović, S. Gudić, M. Kliškić, E.E. Oguzie, L. Carev, Inhibition of copper corrosion in NaCl solution by caffeic acid, Int. J. Electrochem. Sci. 11 (2016) 459–474, https://doi.org/10.1016/S1452-3981(23)15857-3.
[112] J.O'M. Bockris, D.A.J. Swinkels, Adsorption of n-decylamine on solid metal electrodes, J. Electrochem. Soc. 111 (1964) 736, https://doi.org/10.1149/1.2426222.
[113] S. Sharma, A. Kumar, Recent advances in metallic corrosion inhibition: a review, J. Mol. Liq. 322 (2021) 114862, https://doi.org/10.1016/j.molliq.2020.114862.
[114] J. Li, C.W. Du, Z.Y. Liu, X.G. Li, M. Liu, Inhibition film formed by 2-mercapto-benzothiazole on copper surface and its degradation mechanism in sodium chloride solution, Int. J. Electrochem. Sci. 11 (12) (2016) 10690–10705, https://doi.org/10.20964/2016.12.46.
[115] G. Ackermann, D. Hesse, P. Volland, Über Eisen(III)-komplexe mit phenolen. IV. Säurekonstanten einiger polyphenole, Z. Anorg. Allg. Chem. 377 (1970) 92–99, https://doi.org/10.1002/zaac.19703770111.
[116] I.B. Obot, D.D. Macdonald, Z.M. Gasem, Density functional theory (DFT) as a powerful tool for designing new organic corrosion inhibitors. Part 1: an overview, Corros. Sci. 99 (2015) 1–30, https://doi.org/10.1016/j.corsci.2015.01.037.
[117] T.A. Taha, A.A. Azab, M.A. Sebak, Glycerol-assisted sol-gel synthesis, optical, and magnetic properties of $NiFe_2O_4$ nanoparticles, J. Mol. Struct. 1181 (2019) 14–18, https://doi.org/10.1016/j.molstruc.2018.12.075.
[118] B. Balkard, R. Nguyen, M.D. Mellaoui, A. Imjjad, R. Oukhrib, C. Len, H. Zejli, Exploring the corrosion potential of three bio-based furan derivatives on mild steel in aqueous HCl solution: an experimental inquiry enhanced by theoretical analysis, ACS Omega 9 (41) (2024) 42520–42535, https://doi.org/10.1021/acsomega.4c06670.
[119] A. Al-Amiery, N.A. Betti, L.M. Shaker, Exploring the effectiveness of 3-chloro-4-morpholin-4-yl-1,2,5-thiadiazole as an eco-friendly corrosion inhibitor for mild steel in HCl solution: experimental and DFT analysis, Results Eng. 24 (2024) 103014, https://doi.org/10.1016/j.rineng.2024.103014.